A Seismo-lineament Study of Magnitude 3.3-5.3 Earthquakes Near Trinidad, Colorado

A Thesis Submitted to the Faculty of

Baylor University

In Partial Fulfillment of the

Requirements for the Degree of

Bachelor of Science in Geology

By Jordan N. Dickinson

Waco, Texas

May 2015

ABSTRACT

A Seismo-lineament Study of Magnitude 3.3-5.3 Earthquakes Near Trinidad, Colorado

Jordan N. Dickinson, B.S.

Committee Chairperson: Vincent S. Cronin, Ph.D.

This study uses the Seismo-Lineament Analysis Method (SLAM) to attempt identification of the ground-surface trace of the fault(s) that produced seven M 3.3-5.3 earthquakes from 2005 through 2011 in the Raton Basin west of Trinidad, Colorado (latitudes 36.83°-37.20°N, longitudes 104.40°-105.00°W). All seven earthquakes have normal or normal-oblique focal mechanisms, and some have multiple solutions. The average nodal-plane strikes for the seven earthquakes we considered are 355°±13° for east-dipping planes and 6°±21° for west-dipping planes, with average dip angles for all of the nodal planes of 48±5°. There are not many faults shown on published geologic maps of this area, none that spatially correlate with the earthquakes we studied, and no active faults. Major tributary streams in this area flow either NE or SE toward the Purgatoire River, which flows east and is the primary drainage. Prominent drainage lineaments that trend N-S are obvious because of their anomalous orientation within this stream network. From Trinidad to ~2 km beyond Weston, at least seven N-S composite lineaments are evident. One or more of the prominent N-S drainage lineaments is inferred to have developed along an active normal fault. A road cut just east of Valdez, ~100 m east of mile-marker 57 along Colorado State Highway 12, exposes a significant down-to-the-east normal fault that is partially obscured by slope wash or shallow landsliding. Seismo-lineaments associated with a M4.9 earthquake on 8/22/2011, and M5.3 and M4 events on

8/23/2011 encompass this fault exposure and have the same east-down sense of normal displacement.

TABLE OF CONTENTS

LIST OF FIGURES

LIST OF TABLES

ACKNOWLEDGMENTS

This study was supported through a grant to Jordan Dickinson from the Colorado Scientific Society. Additional support was provided by the Baylor University Department of Geology. I would like to extend heartfelt gratitude to Dr. Vincent S. Cronin for his guidance and passion in this project. His knowledge and aid were essential to the development of this thesis. I would also like to thank my committee members, Dr. John Dunbar and Dr. Rena Bonem for taking the time to be involved in this work. I appreciate the help of my field assistant, Rebecca Davis, for not only her time but also for enduring the unfavorable weather in the field. Finally, to my parents, for continuing to support and encourage me throughout my education at Baylor University, I am extremely grateful.

CHAPTER ONE

Introduction

The state of Colorado has surprisingly few active faults, and has had fewer earthquakes than one would expect for such a mountainous area. The online earthquake catalog of the US Geological Survey contains 137 earthquakes with magnitude ≥ 3.0 that occurred in Colorado since 1960 (http://earthquake.usgs.gov/earthquakes/search/). Of these, just one had a magnitude of 5 or greater (M 5.3 on 8/23/2011), fifteen ranged from M 4.0-4.7, and the rest were less than M 4.0. The M 5.3 event and six of the M 4.0 earthquakes occurred in the Raton Basin of south-central Colorado, along the border with New Mexico and just east of Trinidad, Colorado (Figure 1). No other part of Colorado has a similar cluster of earthquakes, and no faults in this area are included in the Quaternary Fault and Fold Database of the United States (http://earthquake.usgs.gov/hazards/qfaults/map/).

The Seismo-Lineament Analysis Method (SLAM) was developed to use earthquake focal mechanism solutions to help locate seismogenic faults (Cronin et al., 2008; Cronin, 2014). Each nodal plane of a given focal mechanism is projected from the hypocenter upward to the ground surface, as represented by a digital elevation model (DEM), plus-or-minus uncertainties in hypocenter location and nodal-plane orientation. The result is a swath projected onto the ground surface that defines the area within which the ground-surface trace of the causative fault would be located if the earthquake is well located, the focal mechanism is accurate, and the fault is approximately planar and emergent at the surface. The larger earthquakes of the Raton Basin are good candidates for investigation using SLAM.

I selected a study area in the Raton Basin bounded by latitudes 36.83°-37.20°N and longitudes 104.40°-105.00°W, which includes parts of southern Colorado and northern New Mexico (Figure 1). The USGS catalog includes 103 earthquakes with epicenters reported within this geographic box since 1960: 2 with M ≥ 5.0 and 9 with magnitudes from 4.0 to 4.9. All except the M 4.2 earthquake of 9/23/1973 have occurred since 2000.

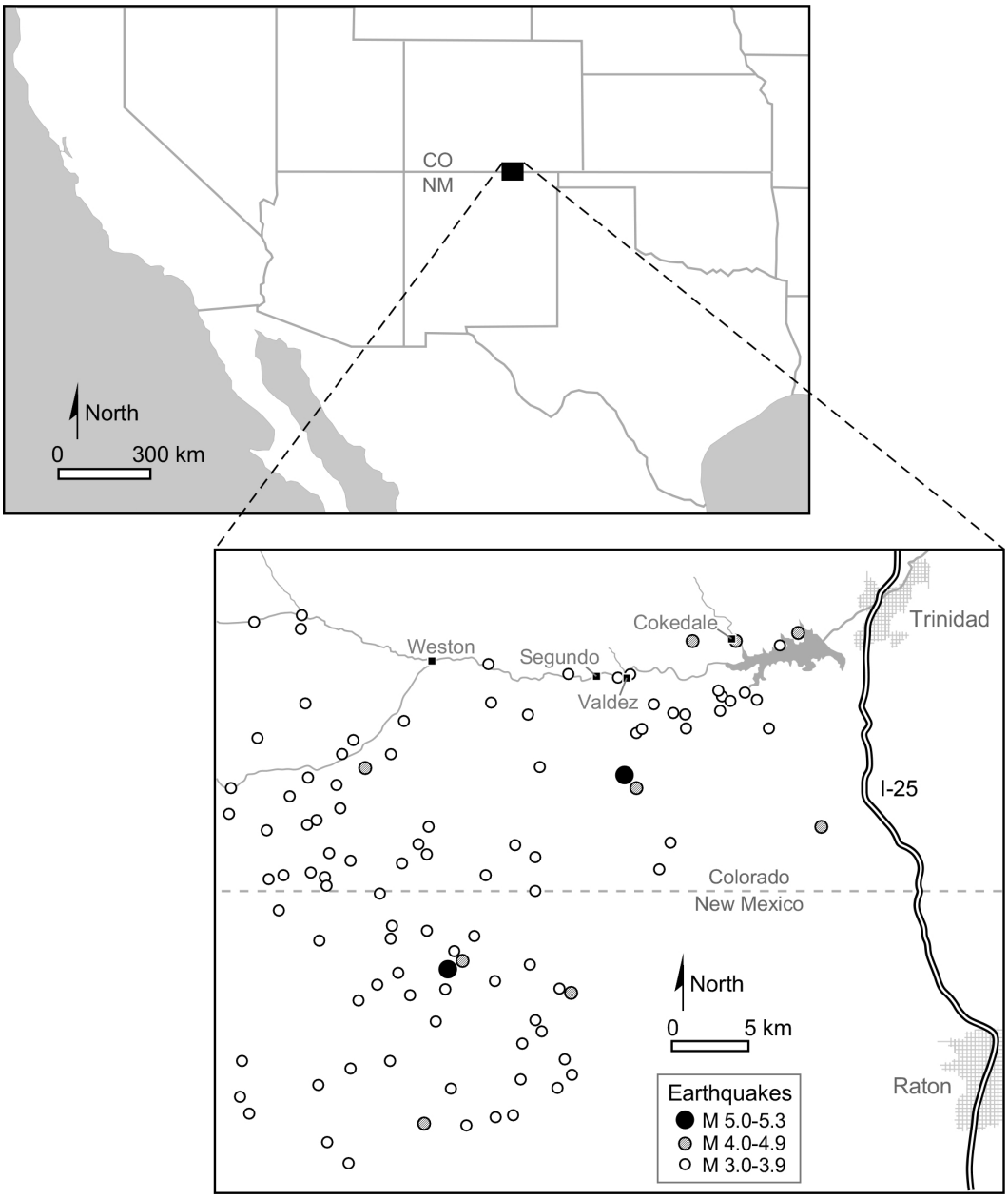

Figure 1. Location map of the study area. The lower map provides detail of the study area, including epicenters of M ≥ 3.0 earthquakes since 1960 reported by the USGS.

None of these events have been associated with ground-surface rupture and none has been attributed to any fault that has been identified in a published map. Significant damage was reported after the M 5.3 earthquake of 22 August 2011 (Matthews, 2012). The losses included damage to buildings in Segundo and Valdez, and lesser damage in Cokedale and Trinidad. There were no reported injuries. Total losses were estimated at $100,000, and included damage to forty-six structures and the destruction of two homes (Matthews, 2012; Morgan and Morgan, 2011).

Focal mechanism solutions have been published for seven of the earthquakes reported in the Raton Basin (Table 1). More than one focal mechanism has been published for four of these events. All of these mechanisms are consistent with normal or normal-oblique faulting on fault surfaces that generally strike north to northeast. Matthews (2012; Meremonte et al., 2002) indicated that earthquake swarms in 2001 and 2011 are clustered along elongate zones that trend northeast, crossing the Puratoire River Valley and Colorado Highway 12 near Segundo and Valdez.

Table 1. Earthquakes with published focal mechanism solutions used in this thesis.

Year	Month	Day	Hr	Min	Sec	Lat	Long	Depth	Mag	Mult Solns?
2005	08	10	22	08	23	36.9-95°	-104.78-79°	12-17 km	4.9-5.0	yes, 3
2007	01	03	14	34	40	36.95°	-104.81°	10	4.4	no
2007	06	09	10	45	45	36.93°	-104.79°	1	3.3	no
2011	05	09	23	28	53	37.14°	-104.84°	10	3.3	no
2011	08	22	23	30	20	37.03-08°	-104.55-65°	5-13.4	4.7-4.9	yes, 3
2011	08	23	05	46	18-21	37.06-21°	-104.59-70°	4-12	5.3-5.4	yes, 3
2011	08	23	14	11	12-13	37.06-07°	-104.69-75°	5-10	4.0	yes, 2

Data are from the ISC Catalog, accessed online via http://colossus.iris.washington.edu in 2014.

Studies of earthquakes with epicenters in the Raton Basin from 2001 through 2013 indicate that there is a likely correspondence between seismicity and fluid injection associated with the extraction of coal-bed methane (Rubinstein et al., 2014; Barnhart et al., 2014). Those studies indicated the existence of a previously unmapped normal fault in Precambrian crystalline basement, striking approximately NE-SW. Robson and Banta (1987) also postulated the existence of basement faults under the sedimentary sequence, but did not indicate that those faults are emergent. Johnson (1969) included several small normal faults on his geologic map of the Trinidad quadrangle (Fig. 2); however, these were not obviously related to any of the recent earthquakes. Meremonte et al. (2002) and Matthews (2012) of the Colorado Geological Survey also described the recent earthquakes and associated damage, but did not ascribe them to a specific fault observed at the ground surface.

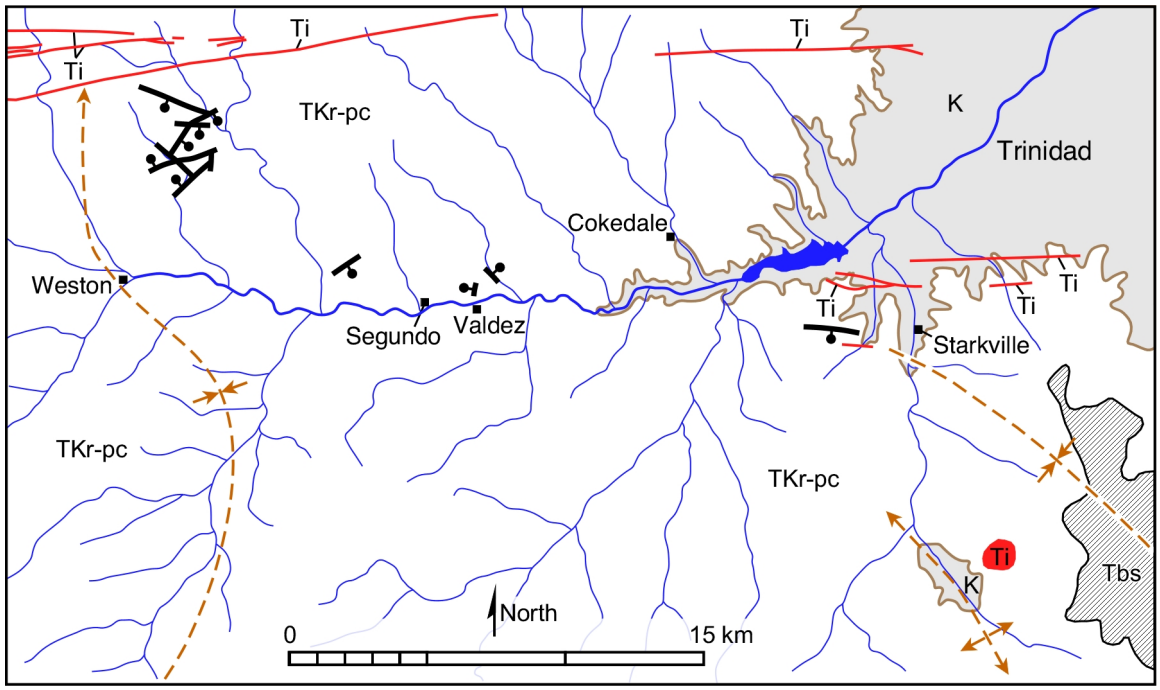

Figure 2. Structural and geologic sketch map of the Colorado portion of the study area. Ti = Tertiary igneous dikes and stocks, K = Cretaceous strata, TKr-pc = Tertiary Raton Formation and Poison Canyon Formation, and Tbs = Tertiary basalt flows. After Johnson, 1969.

The Raton Basin is approximately 150 km long and 75 km wide in current extent, and formed during the Laramide Orogeny (Cooper et al., 2006; Rubenstein et al., 2014). According to mapping in the Trinidad Quandrangle by Johnson (1969; Johnson and Wood, 1956), the sedimentary strata in the Raton Basin include the Cretaceous-aged Pierre Shale, Trinidad Sandstone, and Vermejo Formation consisting of shale, siltsone, sandstone and coal. The Cretaceous-Paleogene boundary and its well-defined boundary layer is near the base of the Raton Formation, which is a sequence of sandstone, shale, and coal overlying a basal conglomerate. The Paleocene-aged Poison Canyon Formation overlies the Raton Formation, and is overlain on the mesas on the southeast side of the study area by Miocene-Pliocene (?) basaltic flows. The Raton and Poison Canyon Formations are intruded by younger igneous dikes and sills.

The purpose of this thesis is to apply SLAM to the focal mechanism solutions of seven magnitude 3.3-5.3 earthquakes reported in the Raton Basin, as a reconnaissance tool to help locate the ground-surface trace(s) of the fault(s) that generated these earthquakes. A better understanding of seismogenic structures in the area is likely to be useful for earthquake risk assessment associated with the Lake Trinidad dam structure and the town of Trinidad, located just downstream.

CHAPTER TWO

Methods

Selection of Study Area

The geographic area chosen for this study was largely dictated by the epicenter locations of the seven earthquakes that were to be studied. Funding from the Colorado Scientific Society and the presence of a reasonably extensive road network on the Colorado side of the border with New Mexico caused much of the effort to be focused on the Purgatoire River Valley along Colorado Highway 12, just east of Trinidad, Colorado (Figure 3). There is a mix of public and private lands in this area, providing acceptable access for a preliminary field study. The Trinidad Quadrangle had been mapped by Johnson (1969), and other geologic resources were available for the area (Cooper et al., 2006; Johnson and Wood, 1956; Matthews, 2012; Meremonte et al., 2002; Morgan and Morgan, 2011; Robson and Banta, 1987; Rubenstein et al., 2014).

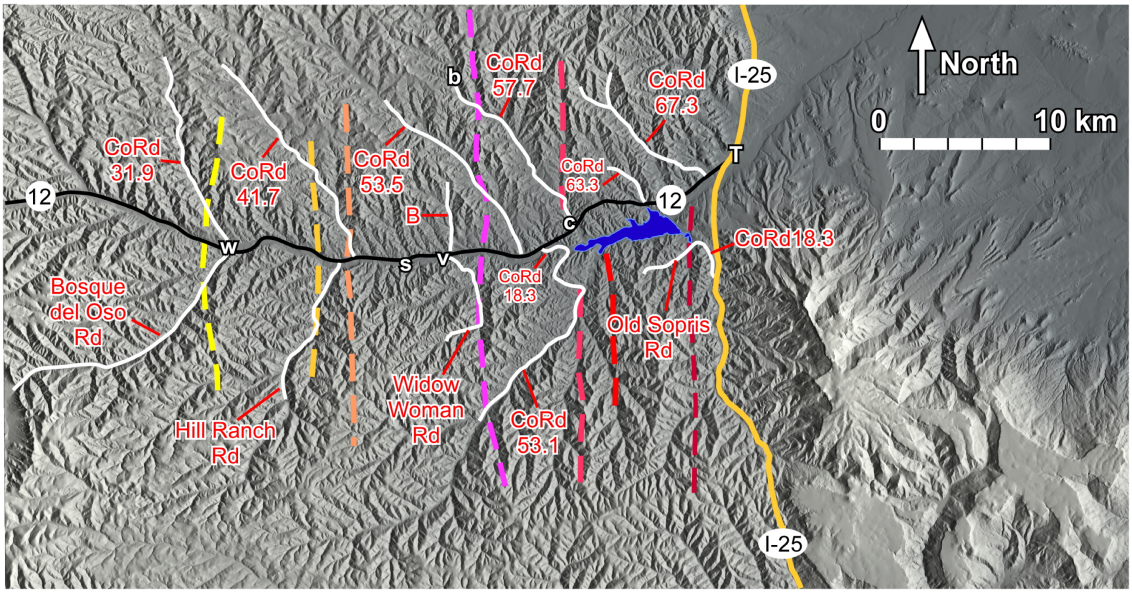

b=Boncarbo c=Cokedale s=Segundo T=Trinidad v=Valdez w=Weston

Figure 3. DEM of the study area. Roads are included and dashed lines are along selected geomorphic lineaments.

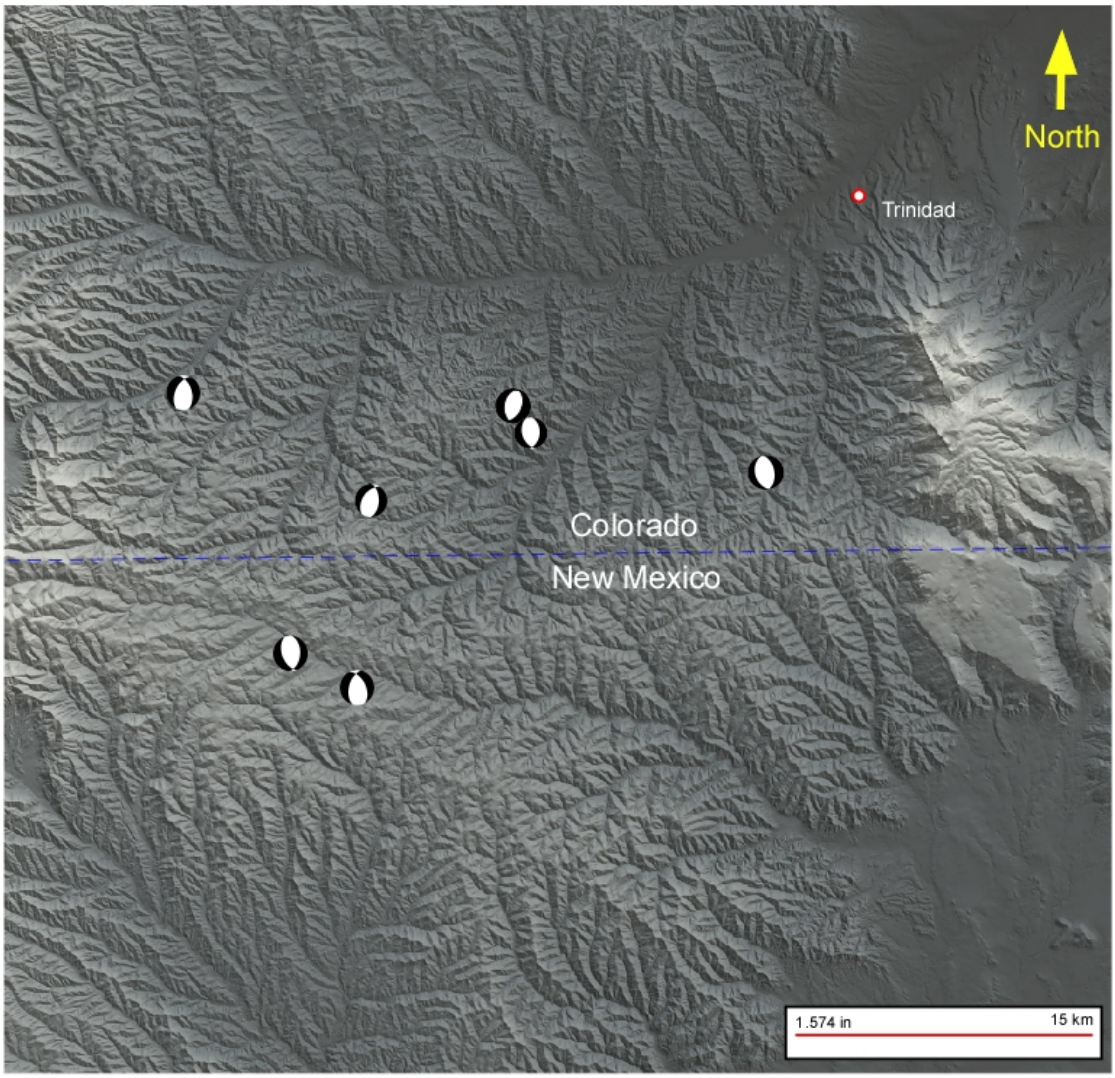

Figure 4. Map showing earthquake epicenter locations of the seven earthquakes used in this study. Focal mechanism solutions by Cronin.

Acquisition of Earthquake Data

Earthquake hypocenters and focal mechanism solutions used in this thesis were obtained from the International Seismological Centre Bulletin (ISC, 2015) using their online search portal (http://isc-mirror.iris.washington.edu/iscbulletin/search/catalogue/) or from the USGS (http://earthquake.usgs.gov/earthquakes/search/). The search was limited to earthquakes with a reported magnitude of at least 3, and epicenters within the

geographic box of this thesis. The SLAM process requires the epicenter location (latitude and longitude), focal depth, and the orientation of both nodal planes from a focal mechanism (Tables 2 and 3). It is strongly preferred to have formal estimates of the uncertainties in all of these parameters. In this thesis, the triaxial uncertainties in the hypocenter location were generally available (Table 2), but uncertainties in nodal plane orientation were not.

DEM Acquisition and Conversion

Digital elevation data for the study area in Colorado and New Mexico were downloaded from the National Map Viewer hosted by the USGS at http://viewer.nationalmap.gov/viewer/ by inputting the bounding coordinates of the study area. The DEMs with the highest resolution that were available for this study have a resolution of 1/3 arc-second, or approximately 9 meters per pixel. The DEM files are acquired in ArcGrid format, and was subsequently converted to an ASCII file using ArcMap. The DEM data format used in the SLAM code is described in Cronin et al. (2008). This DEM file can be thinned and cropped to the desired specifications using *Mathmatica* codes written by Dr. Vince Cronin, that are accessible via http://croninprojects.org/ Vince/SLAM/CurrentBaseCodes.html. A description of the steps used for this analysis is available at http://croninprojects.org/Vince/SLAM/SLAMWorkflow.html.

Seismo-Lineament Analysis

The Seismo-Lineament Analysis Method or SLAM has been described by Cronin et al. (2008), Cronin (2014) and in several Masters theses (*e.g.,* Lancaster, 2011;

Lindsay, 2012; Millard, 2007; Reed, 2014; Seidman, 2007). Each focal plane from an earthquake focal mechanism is projected from the hypocenter upward to the ground surface, which is represented by a DEM. The plane is projected from points tangent to the triaxial ellipsoid that envelops the location-

Table 2. Location and magnitude data for earthquakes used in this thesis

Earthquake Number	Date ID yyMMddhhmm	Latitude °	Longitude °	Depth (km)	Major Horiz Uncert (km)	Minor Horiz Uncert (km)	Azimuth of Major Horiz Uncert	Vertical Uncert (km)	Magnitude
1A	200508102208	36.9	-104.79	12	2.224	2.224	0	5	5
1B	200508102208	36.9489	-104.7904	10	3.339	2.211	41	5	4.9
1C	200508102208	36.92	-104.776	16.7	3	2.1	19	2.7	4.9
2	200701031434	36.948	-104.8083	10	3.613	2.844	138	5	4.4
3	200706091045	36.929	-104.793	1	9.1	7.2	61	5	3.3
4	201105092328	37.138	-104.8401	10	3.31	3.04	19	5	3.7
5A	201108222330	37.0389	-104.6316	12	3.558	3.04	44	5.04	4.9
5B	201108222330	37.032	-104.554	5	3	2.2	203	5	4.7
5C	201108222330	37.08	-104.65	13.4	3.6	3.1	55	5	4.9
6A	201108230546	37.068	-104.6482	10	2.967	1.968	21	5	5.3
6B	201108230546	37.12	-104.59	12	1.112	1.112	0	5	5.3
6C	201108230546	37.063	-104.701	4	9.1	6.4	86	1.8	5.3
6D	201108230546	37.063	-104.701	12	0	0	0	0	5.4
7A	201108231411	37.0658	-104.7546	10	4.374	3.157	28	5	4
7B	201108231411	37.055	-104.692	5	5.3	4.4	87	5	4

Data from ISC Bulletin online event-data search portal, http://isc-mirror.iris.washington.edu/iscbulletin/search/catalogue/

Table 3. Focal Mechanisms and Source Data

Earthquake Number	Nodal Plane 1			Nodal Plane 2			Uncertainties	Sources
	Dip Direction	Dip Angle	Rake	Dip Direction	Dip Angle	Rake		
1A	94	44	-71	248	49	-107	unspecified	HVRD
1B	80	35	-95	266	55	-87	unspecified	ISC SLM
1C	80	35	-95	266	55	-87	unspecified	EHB SLM
2	73	48	-121	295	50	-60	unspecified	ISC SLM
3	63	48	-121	285	50	-60	unspecified	NEIC SLM
4	92	50	-113	305	45	-65	unspecified	ISC NEIC
5A	83	55	-84	253	35	-99	unspecified	ISC GCMT
5B	82	50	-86	255	40	-95	unspecified	USGS pde
5C	83	55	-84	253	35	-99	unspecified	IRIS GCMT
6A	94	54	-101	293	38	-75	unspecified	ISC GCMT
6B	94	54	-101	293	38	-75	unspecified	IRIS GCMT
6C	111	53	-80	275	38	-103	unspecified	USGS pde
6D	113	47	-79	276	44	-102	unspecified	USGS pde
7A	95	45	-75	254	47	-105	unspecified	ISC NEIC
7B	95	45	-75	254	47	-105	unspecified	NEIC

Data from ISC Bulletin online event-data search portal, http://isc-mirror.iris.washington.edu/iscbulletin/search/catalogue/

uncertainty volume around the hypocenter (Figure 5). As the nodal plane intersects the ground surface, plus-or-minus the location uncertainties, it generates a swath called a seismo-lineament (Figure 6). The ground-surface trace of the fault that generated the earthquake is likely to be found within one of the two seismo-lineaments (each associated with one of the two nodal planes) if [1] the earthquake location is accurate, [2] the focal mechanism is accurate, [3] the causative fault is approximately planar, and [4] the fault is emergent at the ground surface (Cronin et al., 2008). The earthquake being studied does not need to have ruptured the ground surface, but the recorded earthquake is likely to have occurred along an existing fault that has ruptured the ground surface at some time during its extended displacement history.

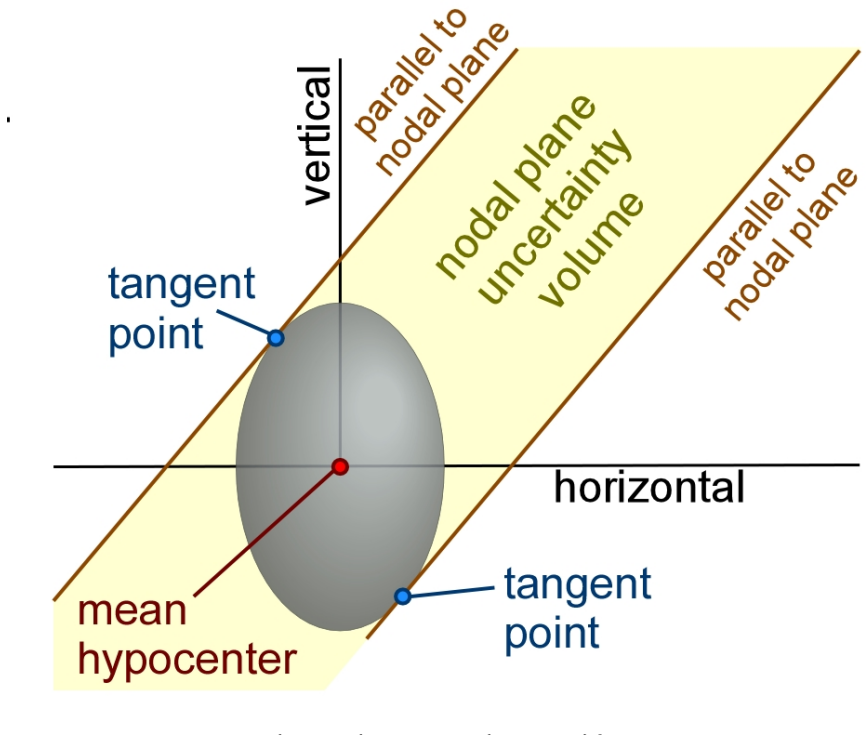

Figure 5. Nodal plane uncertainty volume associated with the hypocenter uncertainty ellipsoid.

The boundaries of each seismo-lineament are calculated using the *Mathematica* code SLAMcode.nb. This thesis research utilized the 2014 version of the SLAM code,

which accommodates a triaxial uncertainty ellipsoid around the hypocenter (Cronin and Cronin, 2014). Once the boundaries are established, a geomorphic analysis is done within the seismo-lineament to identify any lineaments or other features that might have been developed along an active fault.

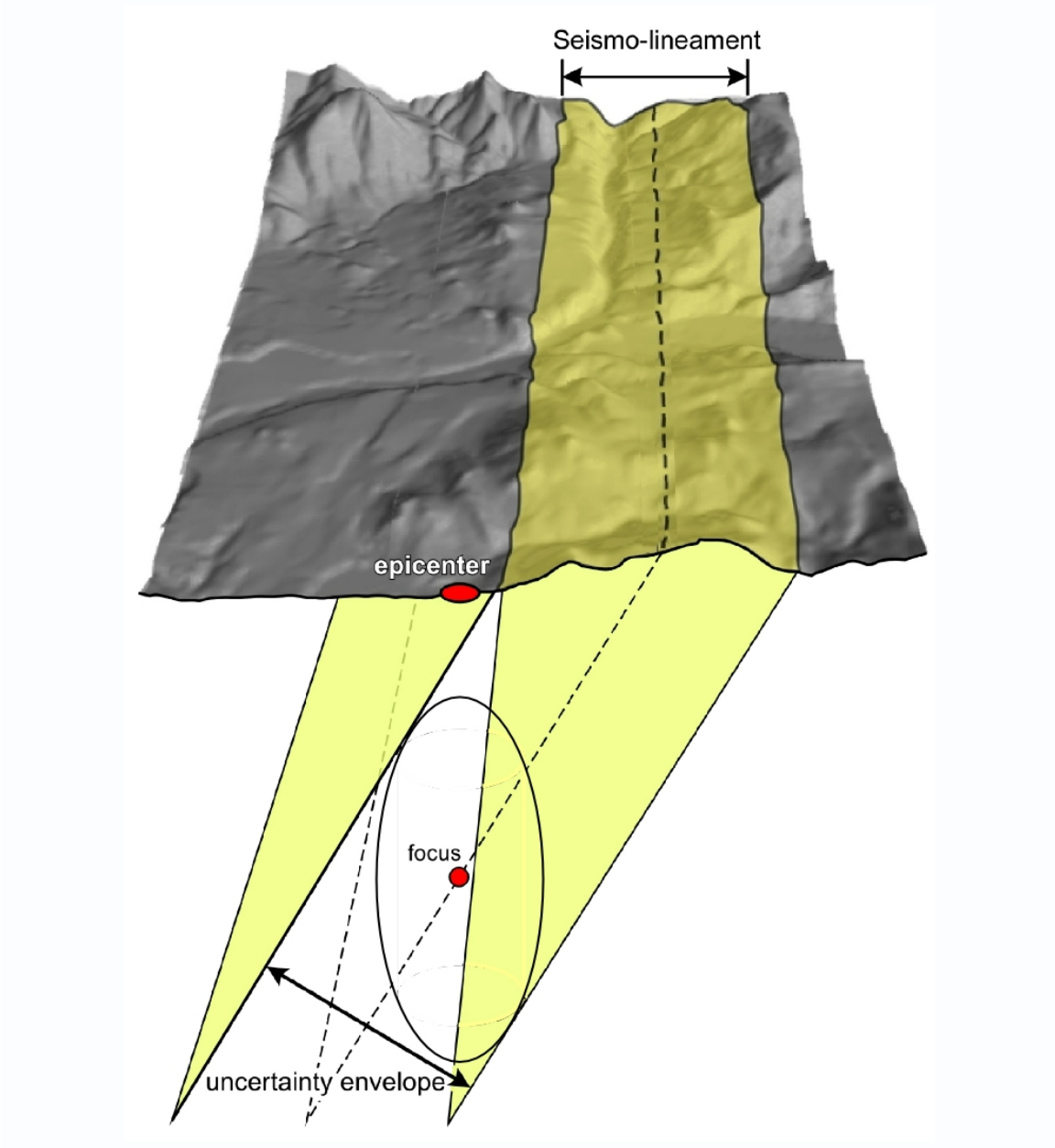

Figure 6. Perspective illustration of seismo-lineament on hillshade surface. The intersection of the ground surface with the uncertainty envelope for a given nodal plane, projected tangent to the uncertainty ellipsoid around the hypocenter, forms the seismo-lineament swath.

Each focal mechanism solution associated with an earthquake event has two nodal planes oriented perpendicular to each other. Nodal planes are planes along which no motion occurred as a result of the first compressional impulse from the earthquake. One of the nodal planes is coincident with the fault that generated the earthquake and is called the fault-plane solution, while the other nodal plane is referred to as the auxiliary plane (Cronin et al., 2008; Cronin, 2010).

The SLAM code displays the boundaries of a given seismo-lineament on a hillshade image constructed using the DEM (Figure 7). The double midline of the swath shows

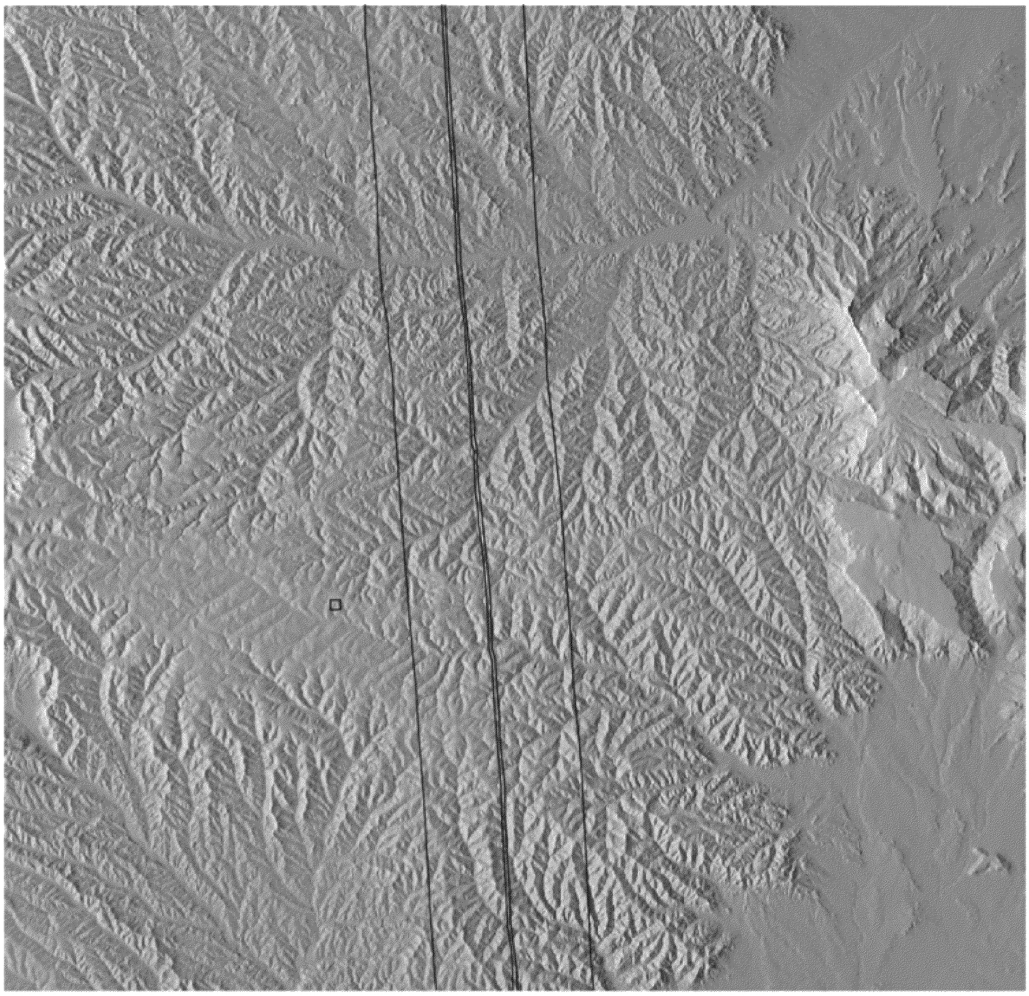

Figure 7. SLAM code raw output for one nodal plane. This output is from the west-dipping nodal plane of earthquake 200508102208B. The small square to the left of the seismo-lineament is the epicenter.

where the nodal plane would intersect the ground surface if it were projected from the mean hypocenter location. The width of the swath is a function of the uncertainty of the location of the earthquake hypocenter as well as the dip angle. As the location uncertainty increases, so does the width of the swath. Additionally, the steeper the dip of the nodal plane is, the narrower the swath. The raw output can then be cleaned up using a graphics application (Figure 8).

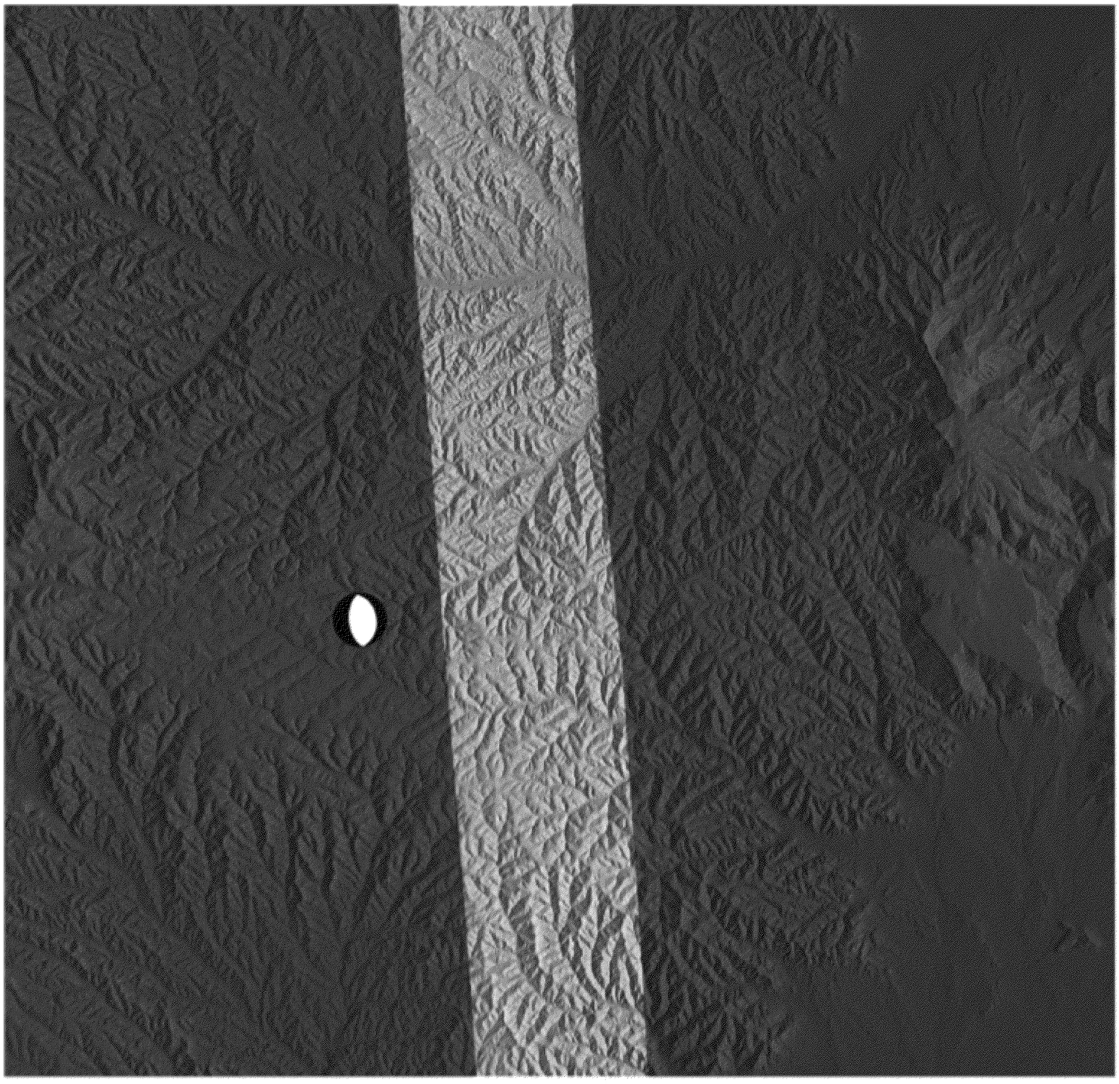

Figure 8. Earthquake seismo-lineament 200508102208B swath with mask applied and focal mechanism solution at the location of the epicenter.

Geomorphic Analysis and Lineaments

The area within each seismo-lineament is illumined at a low incidence angle of perhaps 15° to horizontal, directed perpendicular to the strike of the nodal plane. This modification of the DEM-based hillshade image is performed using the full-resolution (un-thinned) DEM file, processed using the *Mathematica* code *MakeLitHillshade.nb* written by Cronin (http://croninprojects.org/Vince/SLAM/CurrentBaseCodes.html). A hillshade image was used in preference to aerial or orbital photography because a hillshade presents a view of the ground surface without distracting man-made structures or vegetation. When the hillshade is illuminated at a lower angle across the Earth's surface, geomorphic lineaments become prominent (Figure 9).

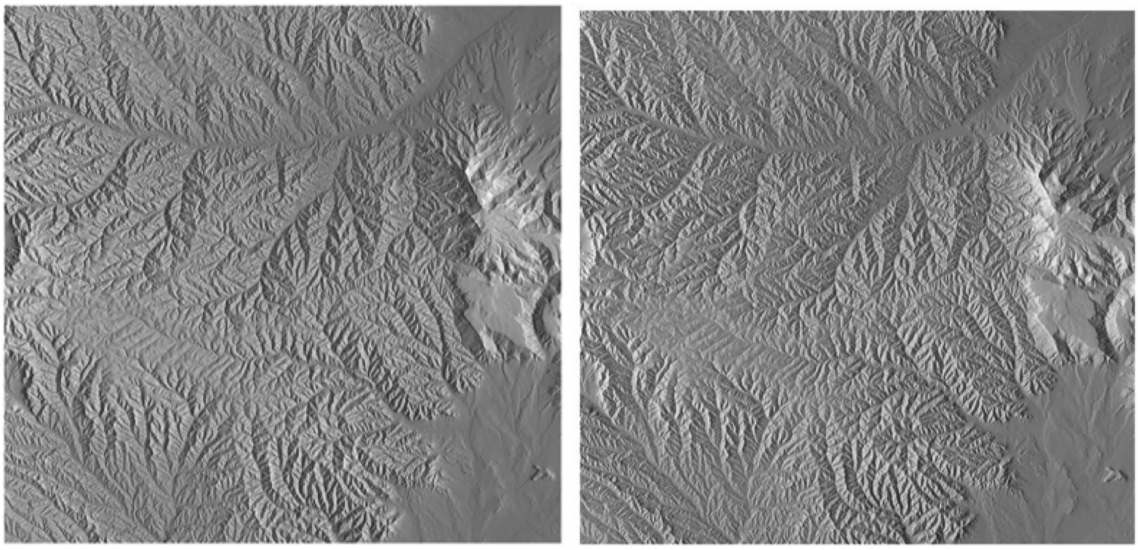

Figure 9. East (right) and West (left) lit hillshade maps of the study area produced in *Mathematica*.

This study used ArcGIS 10 software to analyze 1/3 arc-second DEM-produced hillshade images of the study area to identify geomorphic features. A *geomorphic lineament* is defined by Cronin et al. (1993) as "a long (generally ≥ 5km) collinear or slightly curving array of stream drainage segments or tonal boundaries within the

[hillshade image] that does not appear to be related to human construction or other [human] activities." Faults that propagate up to the ground surface should be identifiable using geomorphic lineaments, which makes searching for exposed ground surface traces of faults in the field easier. Several geomorphic features that could indicate faulting are listed by Cronin and others (2008, after Ray, 1960; Miller, 1961; Wesson et al., 1975; Bonilla, 1982; Slemmons and dePolo, 1986; Cronin et al., 1993; McCalpin, 2009; and Burbank and Anderson, 2001):

- Stream channels that are aligned on opposite sides of a drainage divide;
- Lower-order (smaller) stream channel aligned across a higher-order stream channel;
- An anomalously straight segment of a stream channel;
- Aligned straight segments of one or more stream channels;
- Lower-order stream channel whose trend is directed upstream relative to the higher-order stream it intersects, so water flowing from the smaller stream into the larger stream has to change directions through an obtuse angle;
- Abrupt changes in gradient along a stream channel;
    - A stream channel that steps down in the direction of flow, indicated by rapids or a waterfall (knickpoint);
    - A stream channel that steps up in the direction of flow, indicated by a pond;
- Apparent lateral deflection of an incised stream channel or floodplain;
- Abrupt changes in gradient along a ridge crest;
    - A ridge crest that steps down abruptly in the direction of decreasing elevation;
    - A ridge crest that steps up in the direction of decreasing elevation;
    - A saddle in the ridge crest;
- Apparent lateral deflection of ridge crest;
- Abrupt changes in the gradient of a surface localized along a narrow linear step (fault scarp);
- Benches or faceted spurs at the base of ridges that are apparently unrelated to coastal or fluvial erosion;
- A set of ridges in an en echelon array;
- A topographic basin along a linear trough (pull-apart basin, sag pond);
- A topographic hill along a linear trough (pop-up, pressure ridge); and
- A ridge across the mouth of a stream drainage that is not a glacial moraine (shutter ridge).

Fieldwork

The geomorphic analysis of seismo-lineaments provides the equivalent of a set of hypotheses for where to look for the ground-surface trace of a seismogenic fault. Those hypotheses are subsequently tested through fieldwork whose aim is to find faults that might spatially correlate with the earthquake focal mechanism. Maps of geomorphic lineaments were prepared that included roads and trails, to make fieldwork more efficient (*e.g.*, Figure 2). We used Google Earth to find the latitude and longitude of high-interest sites that could then be located in the field with the use of a hand-held GPS receiver. Some of the roads were private or gated roads, restricting or preventing access. We obtained permission from the homeowners' association to travel on Widow Woman Road to the south of Valdez.

I spent four full days in the field during July of 2014, assisted by Rebecca Davis and, for three of the days, by Connor Cronin and Vince Cronin. The goal of this field season was to locate ground surface exposures of faults within the lineament boundaries. Strike, dip, and orientation data were measured in order to determine which nodal plane was represented once a fault was located. Additional data including GPS location, physical description of the rock unit, lithology on both sides, photographs, orientation of any shear striations, basic description of the fault, and measurement of fault offset with uncertainties were recorded at each possible fault exposure. When faults were discovered, they were photographed and excavated to better measure strike, dip, and rake using a Brunton compass (Figure 10). An aluminum plate was used to extend the surface if the measurements could not be taken directly on the fault wall.

Figure 10. Collecting data at the County Road 41.7 Fault.

CHAPTER THREE

Results

Earthquakes

Data were obtained from the ISC (2015) for seven earthquakes of reported magnitudes greater than 3.0 that occurred within the study area between 2005 and 2011 (Table 2 and Table 3). Some of these earthquake events have only one focal mechanism solution; however, four of them have two or more solutions. The focal depths were reported to be from 1.0 km to 16.7 km below sea level, though the majority of the earthquakes had focal depths greater than or equal to 10.0 km. A few earthquakes had multiple reported depths, such as Earthquake 5 which had reported depths of 12.0 km (ISC [GCMT]), 5.0 km (ISC [NEIC]), and 13.4 km (IRIS [GCMT]). Ground surface elevation in the study area ranges approximately from a low of 1.83 km to a high of 2.78 km, so even the more shallow focal depths are still at least 3.0 km below the surface.

The reported magnitudes ranged between M 3.3 to M 5.3 and averaged around M 4.35. The focal mechanism solutions used in this thesis were provided to the ISC by Harvard University, the USGS National Earthquake Information Center (NEIC), Saint Louis University, and the Global CMT Project. Each of the focal mechanisms in Table 3 indicates normal or normal-oblique faulting as the origin of the earthquake events. The average nodal-plane strikes for the seven earthquakes we considered are 355°±13° for east-dipping planes and 6°±21° for west-dipping planes, with average dip angles for all of the nodal planes of 48±5°.

Seismo-Lineament Analysis

I analyzed 23 seismo-lineaments within the study area, associated with the nodal planes from earthquakes 1-7 (Tables 1-3), which can also be identified using their date-time ID (yyyyMMddhhmm). Although each focal mechanism yields only two nodal planes, some of the earthquakes used in this thesis have multiple published focal mechanism solutions, resulting in additional seismo-lineament swaths. Not all of the seismo-lineaments were within the geographic boundaries established for this thesis, and so were not investigated further. All seismo-lineaments and associated geomorphic lineaments are presented in Appendix A.

The seismo-lineament swaths tend to trend approximately north-south across the Purgatoire River Valley, although there are some exceptions. All of the earthquakes were generated from either normal or normal-oblique faulting, a characteristic that is reflected in the orientation of the two swaths for a given earthquake. For example, if an earthquake were produced by a strike-slip fault, then the SLAM generated swaths should be perpendicular to each other. Seismo-lineaments for a pure dip-slip fault, whether normal or reverse, would be approximately parallel to each other.

Geomorphic Analysis

The SLAM code input generated 28 seismo-lineament swaths. A swath was not analyzed unless both edges were projected within the geographic constraints of this study. Each of the 23 swaths that fit this criterion was examined for geomorphic lineaments that aligned generally parallel to them. Appendix A displays the assessed geomorphic lineaments. There are three previously mapped faults in this area relevant to

this thesis, all of which were identified by Johnson (1969). These faults coincided with traced geomorphic lineaments.

Field Observations

The objective of this fieldwork was to find and record any evidence of faulting within the areas defined by the seismo-lineament swaths in the area just west of Trinidad, Colorado. Fieldwork for this thesis was completed in the summer season of 2014 for various reasons including academic responsibilities and optimal weather for outdoor observation of seismological traces. This study should be regarded as an introductory evaluation of faulting in the area because much of the locality is covered by vegetation and some sections of the projected lineaments were inaccessible due to private property restrictions.

Observed Faults

Eleven exposed fault surfaces located within the projected seismo-lineament swaths were recognized in the field study area. These fault exposures were associated with four separate sites. In Johnson's 1969 geologic map of the area, only three small faults that correlate with the earthquakes in this thesis are mapped.

The County Road 41.7 Fault is located North of the Purgatoire River between the small towns of Segundo and Weston. The exposure is just to the side of the road at latitude 37.1265 and longitude -104.7665 as well as an elevation of approximately 6634 ft (Figure 10). This fault cuts through shale, coal, and sandstone beds with a minimal damage zone. Net slip was measured to be 283 ±10 cm in the coal layer and 272 ±10 cm in the sandstone layer. County Road 41.7 Fault is significant and aligns with a projected

lineament, but dips in the opposite direction of the other lineaments in this study. The following right-hand-rule orientation data were collected on the County Road 41.7 Fault: 279° (strike), 24° (dip angle); 274°, 31°; 277°, 27°; 271°, 21°; 284°, 32°; 289°, 26°; 286°, 31°; 286°, 33°.

Figure 11. Interpreted photograph of North Road B Faults. Numbers correlate to faults found at this exposure.

The North Road B Faults are a series of five small faults that displace shale and sandstone north of the Purgatoire River just east of the town of Valdez (Figure 11). It should be noted that there are two roads in the area named Road B, one of which is coincident with Co Rd 45.5; however, the faulted outcrop can be found on the Road B just east of Co Rd 43.2. These faults are located at latitude 37.1496°, longitude -104.7019° at an approximate elevation of 6657 ft. The separation on fault 1 was ~30±1

cm, and the right-hand-rule measured orientations were as follows: 320°, 69°; 330°, 62°; 331°, 62°; and 317°, 69°. The separation of fault 2 was ~54.6±2 cm, and measured orientations were: 346°, 39°; 339°, 32°; 349°, 32°; 347°, 45°; 346, 43°; 346°, 68°; and 346°, 71°. The separation of fault 3 was ~78±5 cm, and measured orientations were: 12°, 43°; 7°, 46°; 19°, 64°; 35°, 62°; and 34°, 41°. Fault 4 intersects Fault 3. The measured orientations on fault 4 were: 323°, 40°; 319°, 27°; and 346°, 51°. The separation of fault 5 was ~98±5 cm, and measured orientations were: 329°, 45°; 328°, 41°; 310°, 65°; 296°, 66°; 343°, 51°; and 313°, 55°.

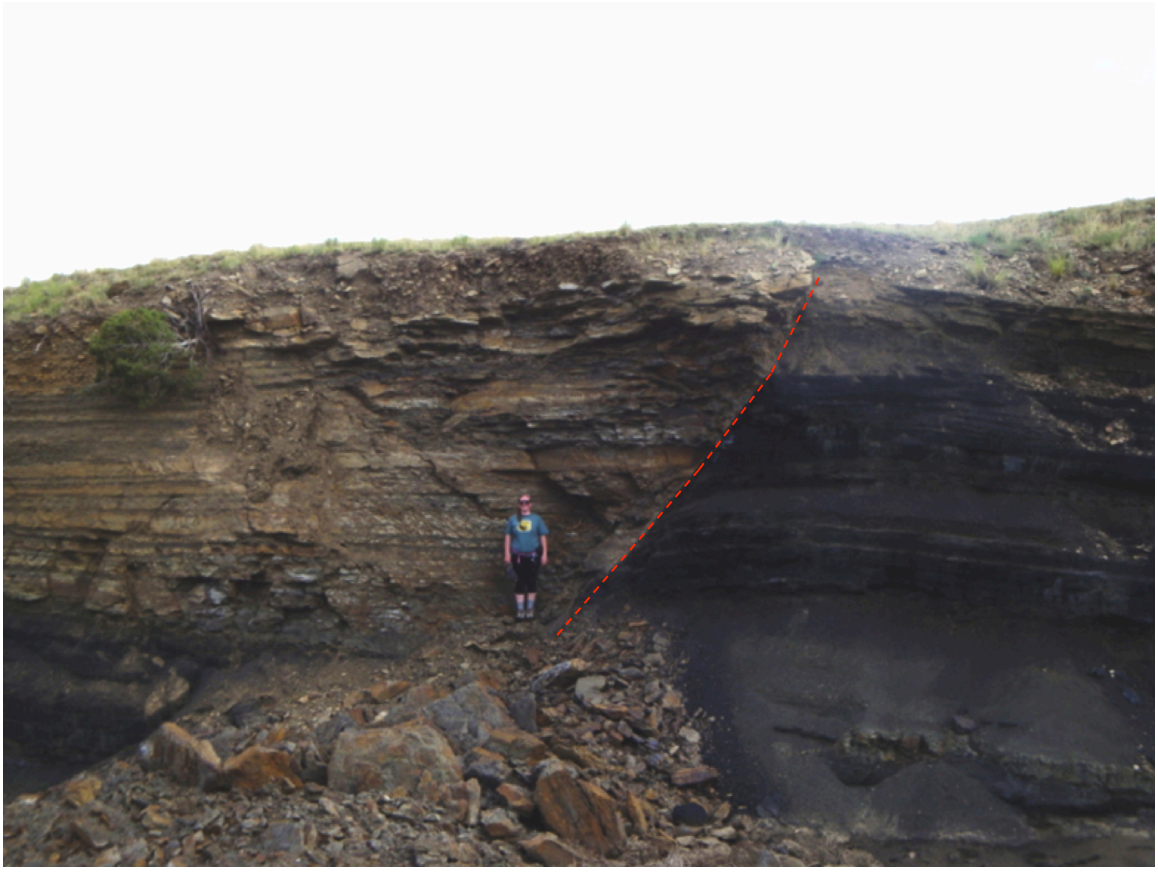

Figure 12. South Road B Fault exposure. Rebecca Davis provides scale.

The South Road B Fault is also located north of the Purgatoire River just east of Valdez and Co Rd 43.2 (Figure 12). The geographic coordinates for this fault are latitude

37.1424°, longitude -104.6976° and elevation ~6515 ft. The South Road B Fault had the largest measured separation of the faults I observed in the area, with approximately 3-4 meters of displacement and an uncertainty of ±0.5 meter. The fault cuts through coal and interbedded shale and sandstone. The measured orientations on the South Road B Fault were: 315°, 44°; 324°, 50°; 297°, 50°; 310°, 45°; and 314°, 45°.

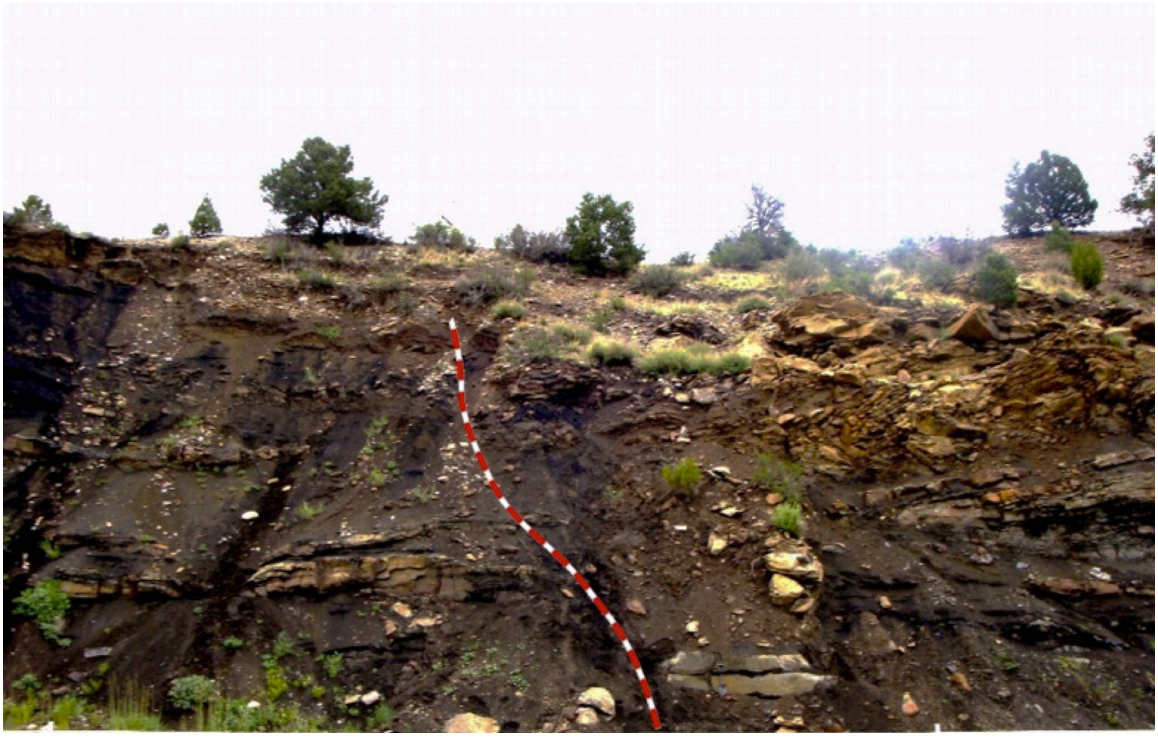

Figure 13. Interpreted photograph of main Highway 12 fault. The main fault dips towards the east.

The Highway 12 Fault is observed on the north side of Colorado State Highway 12 near mile marker 57 (Figure 13). The site is located at latitude 37.1245° and longitude -104.1729°, elevation ~ 6498 ft. Displacement values were not measured at this locality as the feature was partially covered by a landslide and the separation along the fault could not be measured; however, it was an east-dipping normal fault. Orientation data were collected for four faults excavated at the Highway 12 site. Measured right-hand-rule orientations along what was interpreted to be the main faults were 6°, 75°; 5°, 76°; and

342°, 62°. Orientations along minor fault 1 were 183°, 45°; 180°46°; and 201°, 41°. Orientations along minor fault 2 were 344°, 48° and 342° 48°. Orientations along minor fault 3 were 335° 51°; 339° 51°; 334° 49°; 335° 51°; and 330°, 60°.

Geomorphic Features

Although exposed fault surfaces were not found along every geomorphic lineament, geomorphic features were still visible in some places (Figure 14). It is entirely possible that there are fault exposures associated with these lineaments that were inaccessible. These features were still documented in the field because they aligned with a previously mapped geomorphic lineament.

Figure 14. Example of a location where the lineament was still prominent despite a lack of fault features.

CHAPTER FOUR

Discussion and Conclusions

Introduction

This chapter gives initial interpretations of the results produced by this research through the utilization of the SLAM analysis and fieldwork. Additionally, this section will note how future research might fill in the gaps where an absence of data impeded interpretation. Seven earthquakes with no previously known associated faults were analyzed in this thesis. The Purgatoire River valley is not a typical dendritic system. Drainages and tributaries in this system seem to be formed by lithologic or structural controls including faults and joints. Both drainage lineaments that trended with nodal planes and fault exposures were discovered in the field. However, it was not possible to make strong correlations between the faults and earthquakes for several reasons including a limited amount of time in the field, soil and vegetation obscuring most surface traces, and the restrictions of privately owned property.

Existing maps of the area west of Trinidad, Colorado indicate only three small faults and an anticline (Johnson, 1969). Results from this thesis indicate that the previously mapped faults in this region are correctly identified, however there are significantly more seismogenic faults that have not been mapped yet. It is also possible that among the seven earthquake events, several of them might have occurred along the same fault. This hypothesis is further supported by the fact that some of the seismo-lineament swaths from separate earthquakes align or overlap with those of another.

M 4.9-5 Earthquake of August 10, 2005

Only the west dipping nodal planes of the M 4.9-5 earthquake of August 10, 2005 lie fully within the geographic constraints of the study area. The east dipping planes can consequently be considered the auxiliary planes of the focal mechanism. The seismo-lineament of focal mechanism solution B correlates with the Road B faults as well as the Highway 12 Fault; however both of these faults are east dipping faults. This swath also strongly correlates to Widow Woman Canyon, a distinct north to south trending geomorphic lineament that is not associated with any previously mapped fault. I did not find a fault exposed at the ground surface that spatially correlates with this earthquake.

M 4.4 Earthquake of January 3, 2007

The M 4.4 earthquake of January 3, 2007 has only one published focal mechanism solution. Both of the seismo-lineament swaths produced were within the geographic boundaries of the study area. Neither of the seismo-lineaments correlates with any faults observed in the field. The east-dipping nodal plane is located east of Weston where it intersects few roads. Due to limited time, the field area was not surveyed any further than the initial lineament projected just past Weston. It is possible that there is a fault located within this seismo-lineament. The seismo-lineament associated with the west-dipping nodal plane includes a site along Saruche Canyon Road at latitude and longitude (37.1183, -104.5952) where sheared rock was observed along a geomorphic (drainage) lineament (Figure 15). No orientation data were obtained on the inferred fault at this location.

Figure 15. Inferred fault gouge found at Saruche Canyon lineament.

M 3.3 Earthquake of June 9, 2007

The seismo-lineament analysis of the M 3.3 event of 2007 produced swaths that were similar to those delineated by the M 4.4 earthquake of January 3, 2007. These two earthquakes might have been generated by the same fault. The east-dipping nodal plane had several promising geomorphic lineaments contained within its boundaries. However, due to the same constraints limiting the east-dipping nodal plane of the M 4.4 event of 2007, much of this area was not analyzed in the field. The west-dipping lineament swath includes an inaccessible fault on Highway 12 (Figure 16). Johnson (1969) identified a small fault within this seismo-lineament. I infer that the west-dipping nodal plane was the fault plane, and the east-dipping plane was the auxiliary plane.

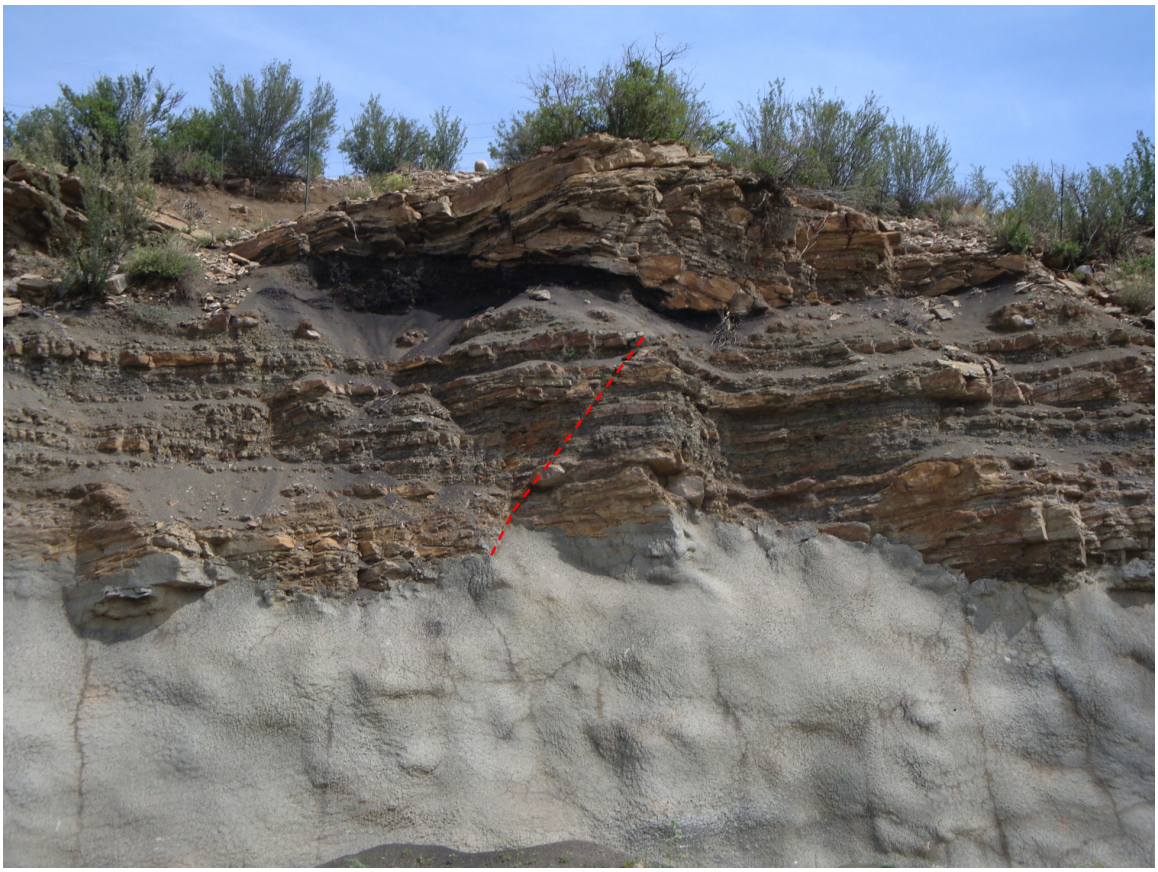

Figure 16. Inaccessible fault on Highway 12 (37.1219, -104.7726) with an estimated net displacement of 6 – 12 inches. The fault dips west.

M 3.7 Earthquake of May 9, 2011

The seismo-lineament analysis of the M 3.7 earthquake of May 9, 2011 rendered only one nodal plane within the geographic constraints of the study. This swath is more closely oriented northeast to southwest rather than north to south. No faults or trends that correlate to this nodal plane were seen in the field and the association between this earthquake and a ground surface feature remains ambiguous. Johnson's (1969) geologic map displays a small fault that is sub-parallel to this swath and might be related. It is likely that an exposure of the fault that generated this earthquake is located in an area that was inaccessible during this field season.

M 4.7-4.9 Earthquake of August 22, 2011

Multiple focal mechanism solutions were published for this event. Both nodal planes projected from focal mechanism solutions A and B, as well as the east-dipping nodal plane from focal mechanism solution C, are located within the study area. The west-dipping nodal planes of A and B have comparatively few geomorphic lineaments and no faults within their boundaries. Focal mechanism solution B's east-dipping nodal plane does not overlap at all with A or C. It does coincide with the Widow Woman Canyon trend as well as the field observed lineament on Saruche Canyon Road that contained possible fault gouge. The small east-dipping fault mapped by Johnson (1969) also appears on the edge of the B lineament. The east-dipping nodal planes of solutions A and C largely coincide with the Highway 12 fault since there is only ~10° difference between their strike measurements (Figure 16). The east to west striking County Road 41.7 Fault is also inside these lineaments. The Highway 12 Fault is spatially correlated with this earthquake event. There is also an inaccessible fault and a location of potential jointing on Highway 12 (Figure 17). I interpret the east-dipping nodal planes for this earthquake event to be fault planes and the west-dipping planes are auxiliary planes.

Figure 17. Jointing on Highway 12, latitude 37.1422°, longitude -104.8562°.

M 5.3 Earthquake of August 23, 2011 5:46 am

Seismo-lineaments computed from three focal mechanisms of the M 5.3 earthquake of August 23, 2011 correspond to several different faults and lineaments within the field. This earthquake event occurred only one day after the M 4.7-4.9 event of August 22, 2011 and was soon followed by another event later the same day. All projected nodal planes are located within the study area and lineaments from focal mechanisms A and B were very similar; however, the swaths produced by solution C are very different and cover a much larger area.

Both west-dipping planes of solutions A and B have no correlation to any faults or lineaments viewed in the field and are interpreted to be the auxiliary planes of their respective solutions. The east-dipping lineament of A includes the geomorphic lineaments of County Road 41.7, the inaccessible Highway 12 Fault, and the possible joint features on Highway 12. Focal mechanism solution B's swath encompasses the east-dipping fault mapped by Johnson (1969) but the strikes are not quite parallel to each other. The east-dipping nodal plane of solution B strongly correlates to the North Road B fault series (Figure 18), the South Road B fault (Figure 19), and the Highway 12 fault. The east-dipping nodal plane of focal mechanism C spatially correlates with Widow Woman Canyon and several of the geomorphic trends observed in the field including those on CO 57.7, Saruche Canyon, and two locations on Highway 12 close to Lake Trinidad. Although it is very dissimilar from the other west-dipping nodal planes produced for this earthquake, the swath is concurrent with Johnson's (1969) east-dipping fault and the inaccessible fault at latitude and longitude 37.1219, -104.7726. The association of this earthquake with a specific fault or trend remains ambiguous because of the placement of its lineament swaths and the differing focal mechanism solutions.

M 4 Earthquake of August 23, 2011 2:11 pm

Seismo-lineaments computed from two focal mechanisms of the M 4 earthquake of August 23, 2011 spatially coincide with several geomorphic trends and faults observed in the field. The west-dipping nodal planes of both focal mechanism solutions are sub parallel to the Widow Woman Canyon trend and have the same orientation as some of the North Road B faults. There are many geomorphic lineaments in the area that coincide with this nodal plane. The east-dipping nodal plane of focal mechanism A contains

possible geomorphic lineaments viewed on Cherry Canyon Rd, CO Road 31.9, and Highway 12, but no faults were observed in the field. Focal mechanism B provided an east-dipping nodal plane that includes at least two prominent geomorphic lineaments and the Highway 12 fault and both Road B faults. A determination of which nodal plane represents the fault plane as well as a spatial correlation to a single fault remains uncertain.

The epicenter locations of the two August 23, 2011 earthquakes are extremely close to each other yet their projected lineaments are rather different. This fact suggests that the afternoon earthquake may not have ruptured along the same fault as the morning event. Furthermore, it is probable that the seismic activity produced by the M 5.3 earthquake triggered the release of energy in the fault that produced the M 4 earthquake. If one takes into account the M 4.7-4.9 event that occurred the day before on August 22, it is possible that particular earthquake set off a sort of chain reaction of energy release along several faults in the region.

Future Research

Further research is needed to expand the results of this thesis and gain a better understanding of the neotectonics of this area. The study area displays potential for fault exposures, although many are currently inaccessible because of their location on private lands. Faults discovered during the field study should be further analyzed for correlations to earthquake events and to each other. Seismo-lineaments not associated with faults in this study could have exposures elsewhere in the area. If the oil and gas companies in the area were to give access and collaborate with the researchers, it is likely that better results

and more fault exposures would be found. Finally, the use of LiDAR surveying may be advantageous in this study area because previously unseen lineaments could be recognized.

REFERENCES

Barnhart, W.D., Benz, H.M., Hayes, G.P., Rubinstein, J.L., and Bergman, E., 2014, Seismological and geodetic constraints on the 2011 M_W 5.3 Trinidad, Colorado earthquake and induced deformation in the Raton Basin, *Journal of Geophysical Research, Solid Earth*, v. 119, p. 7923-7933, doi:10.1002/2014JB011227.

Bonilla, M.G., 1982, Evaluation of potential surface faulting and other tectonic deformation: U.S. Geological Survey Open-File Report 82-732, p. 58.

Burbank, D.W. and R.S. Anderson, 2001, Tectonic Geomorphology: Blackwell Science, Oxford, p. 274.

Cooper, J.R., Crelling, J.C., Rimmer, S.M., Whittington, A.G., 2006, Coal metamorphism by igneous intrusion in the Raton Basin, CO and NM: implications for generation of volatiles, *International Journal of Coal Geology*, 71, pp. 15–27

Cronin, V.S., 2014, Seismo-Lineament Analysis Method (SLAM), using earthquake focal mechanisms to help recognize seismogenic faults, *in* Grutzner, C., Choi, J-H., Edwards, P., and Kim, Y-.S., [editors], *Proceeding of the 5th International INQUA Meeting on Paleoseismology, Active Tectonics and Archeoseismology*, 21-27 September 2014, p. 28-31, ISBN 9791195344109 93450; available via http://CroninProjects.org/Vince/SLAM/CroninINQUA_PATA14.pdf

Cronin, V.S., 2010, A draft primer on focal mechanism solutions for geologists: Teaching Quantitative Skills in the Geosciences, http://serc.carleton.edu/files/ NAGTWorkshops/structure04/Focal_mechanism_primer.pdf.

Cronin, V.S., and Cronin, K.E., 2014, Revised geometry of nodal-plane uncertainty volume used in the seismo-lineament analysis method to locate seismogenic faults: Seismological Society of America Annual Meeting, Anchorage, Alaska, http://www.seismosoc.org/meetings/2014/app/index.html - _14-698.

Cronin, V.S., Millard, M., Seidman, L, and Bayliss, B., 2008, The Seismo-Lineament Analysis Method (SLAM) -- A Reconnaissance Tool to Help Find Seismogenic Faults: Environmental and Engineering Geology, v. 14, no. 3, p. 199-219. Available via GeoScience World at http://eeg.geoscienceworld.org/cgi/content/abstract/14/3/199

Cronin, V.S., Schurter, G., and Sverdrup, K.A., 1993, Preliminary Landsat lineament analysis of the northern Nanga Parbat-Haramosh Massif, northwest Himilaya: Geological Society of London Special Publication, No. 74, p. 193-206.

International Seismological Centre, 2015, On-line Bulletin: International Seismological Centre, Thatcham, United Kingdom, accessed 2014-2015 via http://colossus.iris.washington.edu/iscbulletin/search/.

Johnson, R.B., 1969, Geologic Map of the Trinidad quadrangle south-central Colorado: U.S. Geological Survey: *Geological Investigations Map* I-558, scale 1:250,000; accessible online via http://ngmdb.usgs.gov/Prodesc/proddesc_9346.htm

Johnson, R.B. and Wood, G.H., 1956, Stratigraphy of upper cretaceous and tertiary rocks of Raton Basin, Colorado and New Mexico, *Bulletin of the American Association of Petroleum Geologists*, 40, p. 707-721.

Lancaster, Daniel, 2011, Correlation of earthquakes with seismogenic faults along the Northern Arizona Seismic Belt, southwestern margin of the Colorado Plateau: M.S. thesis, Baylor University, accessible via http://hdl.handle.net/2104/8228.

Lindsay, Ryan, 2012, Seismo-lineament analysis of selected earthquakes in the Tahoe-Truckee area, California and Nevada: M.S. thesis, Baylor University, accessible via http://hdl.handle.net/2104/8441.

Matthews, V., III, 2012, The Trinidad, Colorado earthquakes: Colorado Geological Survey, accessed 20 April 2015 via http://coloradogeologicalsurvey.org/wp-content/uploads/2013/08/Trinidad-2011.pdf

McCalpin, J., ed., 2009, Paleoseismology [2nd edition]: Amsterdam, Academic Press, 613 p.

Meremonte, M.E., Lahr, J.C., Frankel, A.D., Dewey, J.W., Crone, A.J., Overturf, D.E., Carver, D.L., and Bice, D.T., 2002, Investigation of an earthquake swarm near Trinidad, Colorado, August-October 2001, U.S. Geol. Surv. Open-File Rept. 02-0073.

Millard, M., 2007, Linking onshore and offshore data to find seismogenic faults along the Eastern Malibu coastline: M.S. thesis, Baylor University, accessible via http://hdl.handle.net/2104/5109.

Miller, V.C., 1961, Photogeology: McGraw-Hill, New York, p. 248.

Morgan, M.L., and Morgan, K.S., 2011, Preliminary damage report of the August 22, 2011 Mw 5.3 earthquake near Trinidad, Colorado: Colorado Geological Survey, accessed 20 April 2015 via http://coloradogeologicalsurvey.org/geologic-hazards/earthquakes-2/trinidad-earthquakes/

Ray, R.G., 1960, Aerial photographs in geologic interpretation and mapping: U.S. Geological Survey Professional Paper 373, p. 230.

Reed, Tyler, 2014, Spatial correlation of earthquakes with two known and two suspected seismogenic faults, north Tahoe-Truckee area, California: M.S. thesis, Baylor University, accessible via http://hdl.handle.net/2104/9097.

Robson, S., and Banta, E., 1987, Geology and hydrology of deep bedrock aquifers in eastern Colorado, *USGS Water-Resources Investigation Report 85-4240,* 22 pp.; accessible via http://pubs.er.usgs.gov/publication/wri854240

Rubinstein, J.L., Ellsworth, W.L., McGarr, A., and Benz, H.M., 2014, The 2001-present induced earthquake sequence in the Raton Basin of northern New Mexico and southern Colorado, *Bulletin of the Seismological Society of America*, v. 104, no. 5, p. 2162-2181, doi: 10.1785/0120140009.

Seidman, Lauren, 2007, Seismo-lineament analysis of the Malibu Beach quadrangle, Southern California: M.S. thesis, Baylor University, accessible via http://hdl.handle.net/2104/5108.

Slemmons, D.B., and dePolo, C.M., 1986, Evaluation of active faulting and associated hazards, *in* Studies in Geophysics – Active Tectonics: Washington D.C., National Research Council, National Academy Press, p. 45-62.

U.S. Geological Survey, 2015, The National Map Viewer, accessed 2014-2015, from USGS web site: http://viewer.nationalmap.gov/viewer/.

U.S. Geological Survey and Colorado Geological Survey, 2006, Quaternary fault and fold database for the United States, accessed 2014-2015, from USGS web site: http//earthquakes.usgs.gov/regional/qfaults/.

Wesson, R.L., Helley, E.J., Lajoie, K.R. and Wentworth, C.M., 1975, Faults and future earthquakes, in Borcherdt, R.D., [editor], Studies for seismic zonation of the San Francisco Bay region: U.S. Geological Survey Professional Paper 941-A, p. 5-30.

APPENDIX

Geomorphic analysis of seismo-lineaments

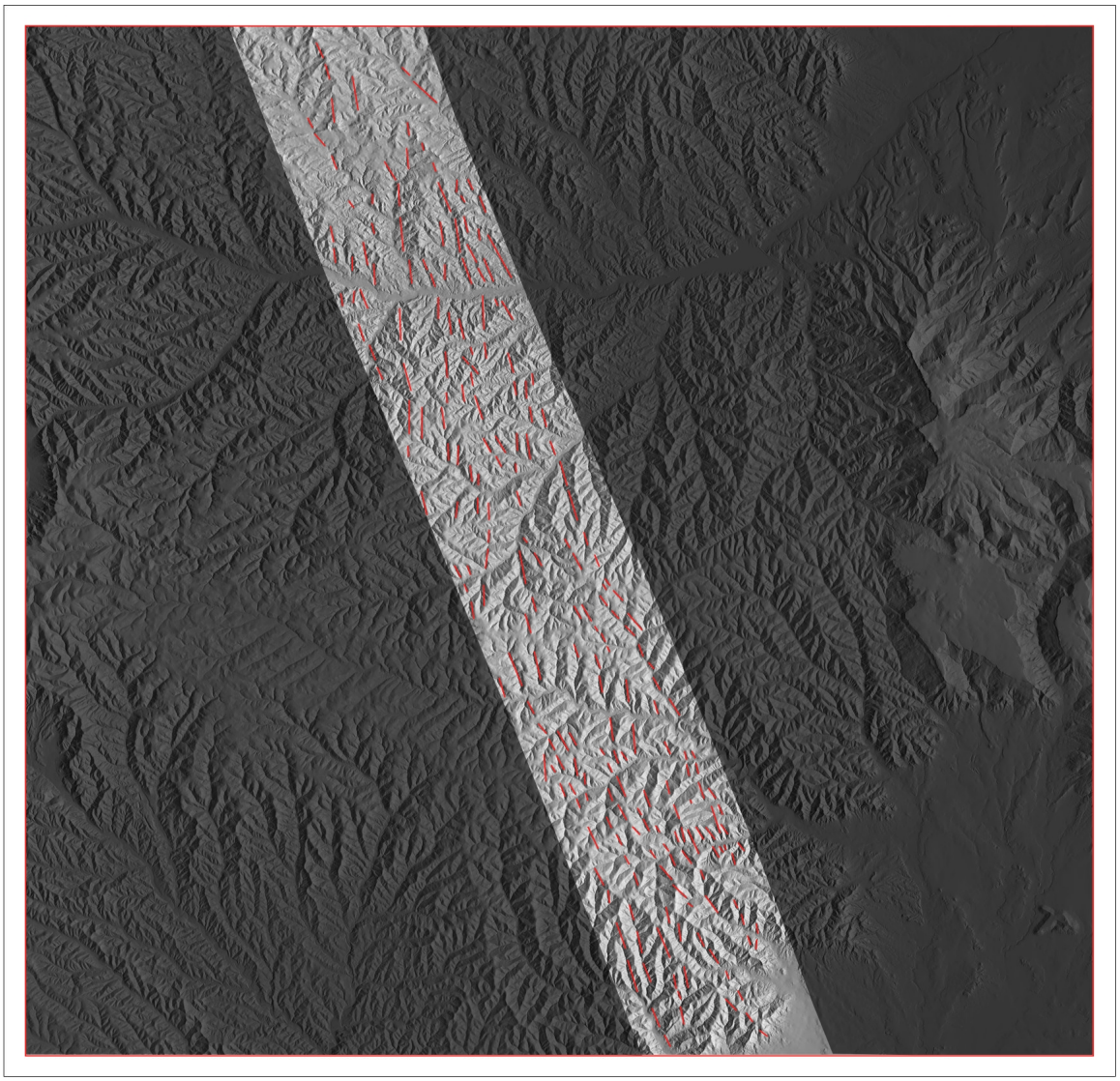

Figure A1. 200508102208A nodal plane 2. Dip direction 248° and dip angle 49°.

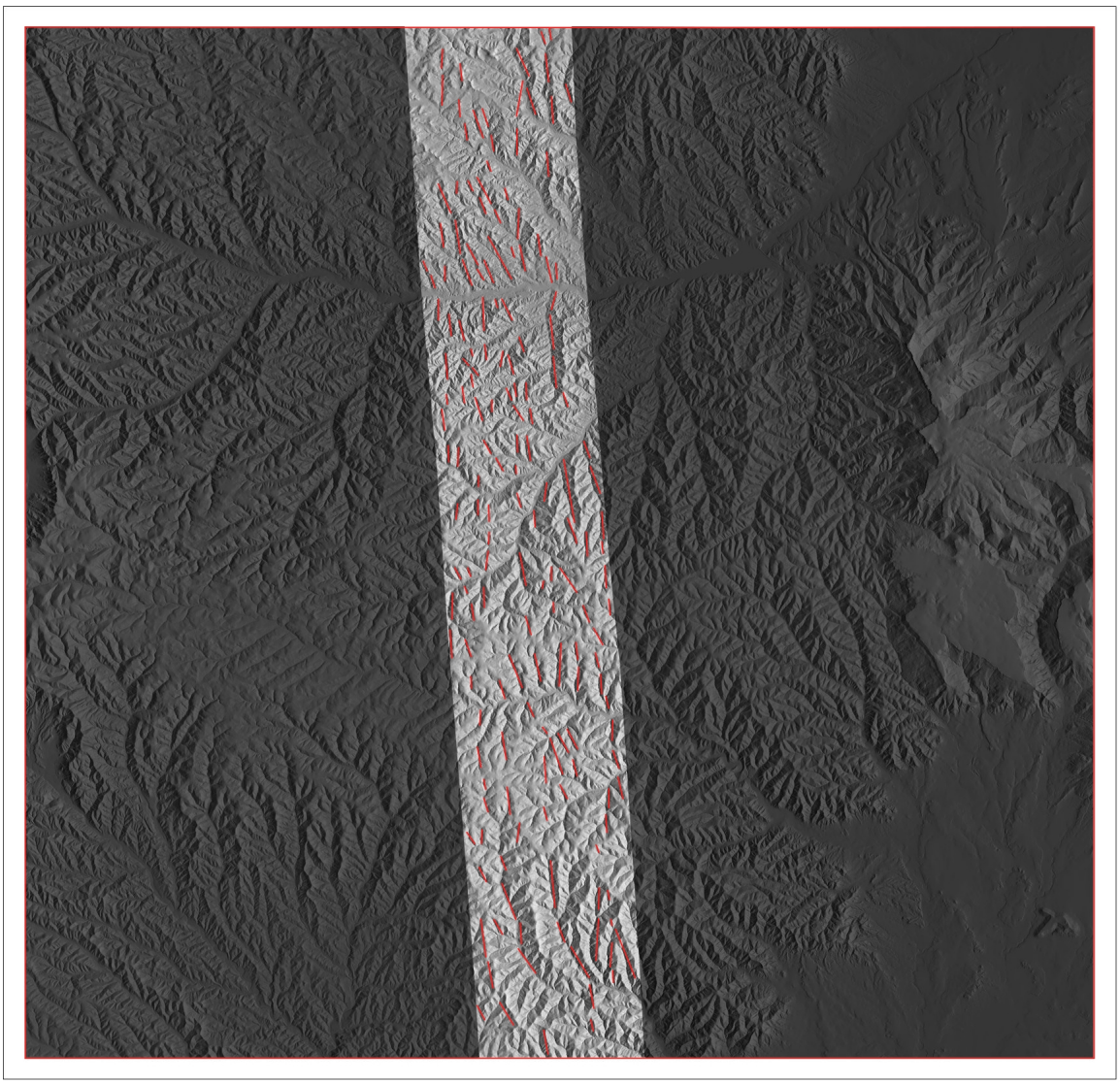

Figure A2. 200508102208B nodal plane 2. Dip direction 266° and dip angle 55°.

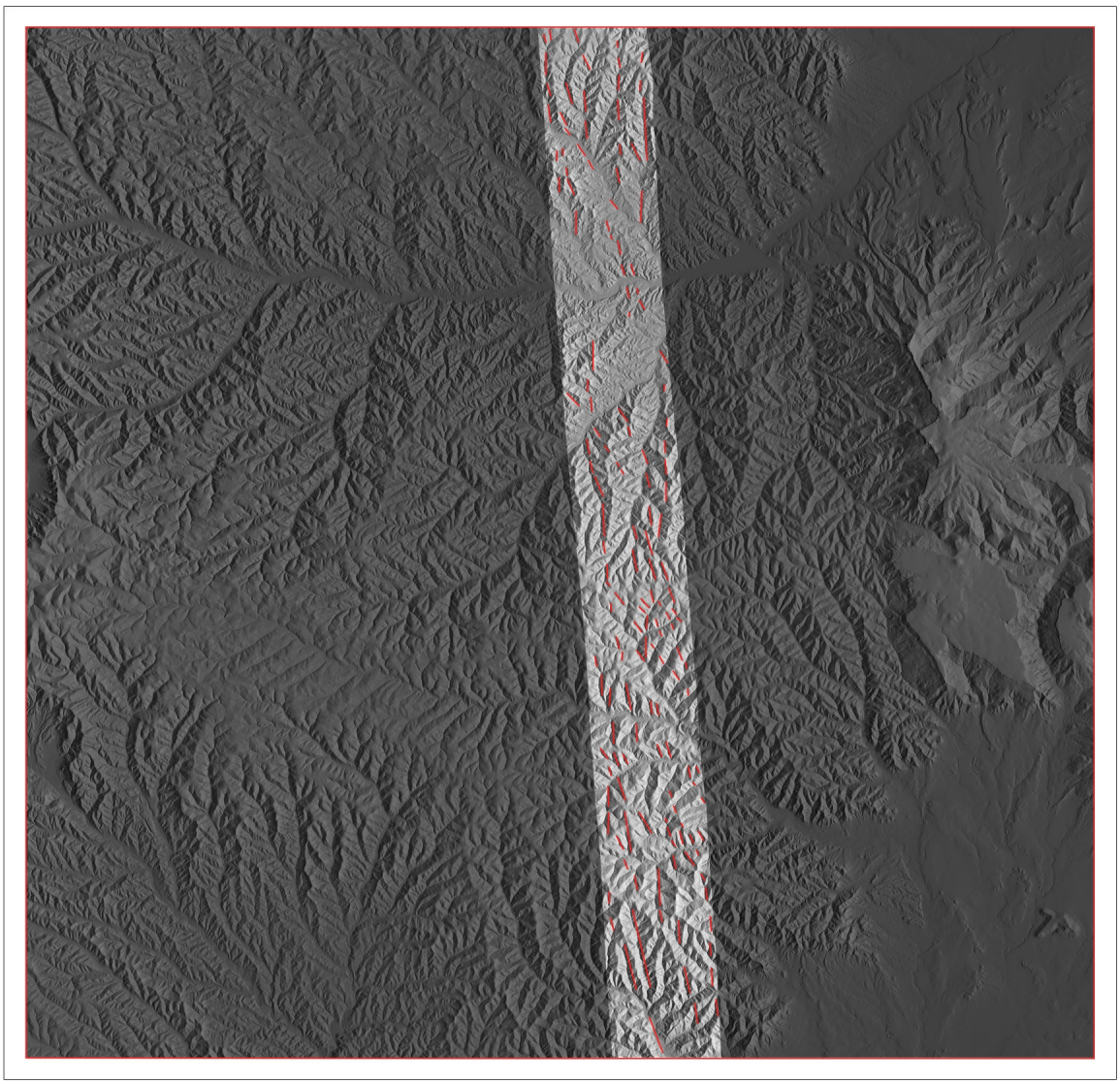

Figure A3. 200508102208C nodal plane 2. Dip direction 266° and dip angle 55°.

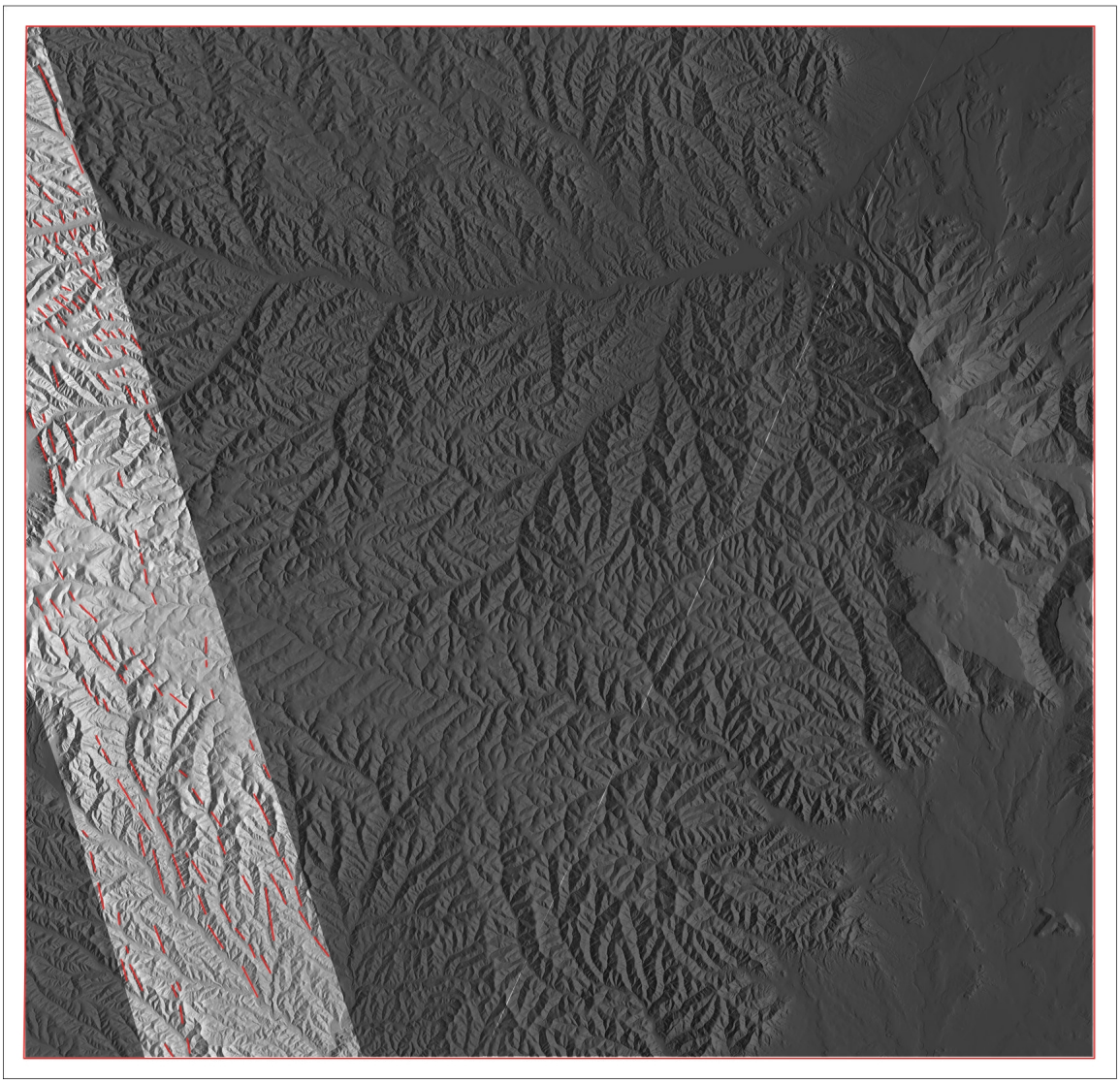

Figure A4. 200701031434A nodal plane 1. Dip direction 73° and dip angle 48°.

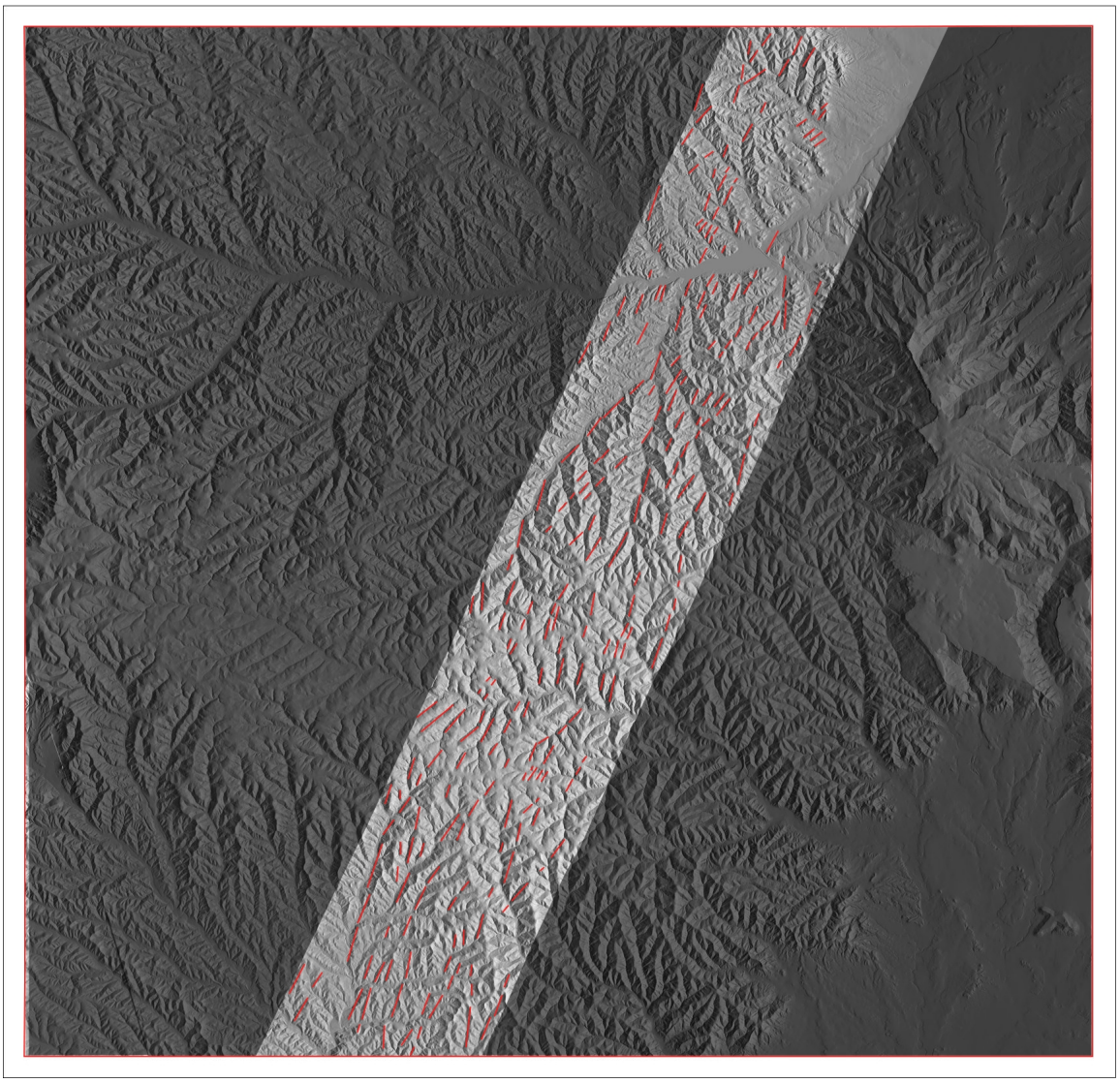

Figure A5. 200701031434A nodal plane 2. Dip direction 295° and dip angle 50°.

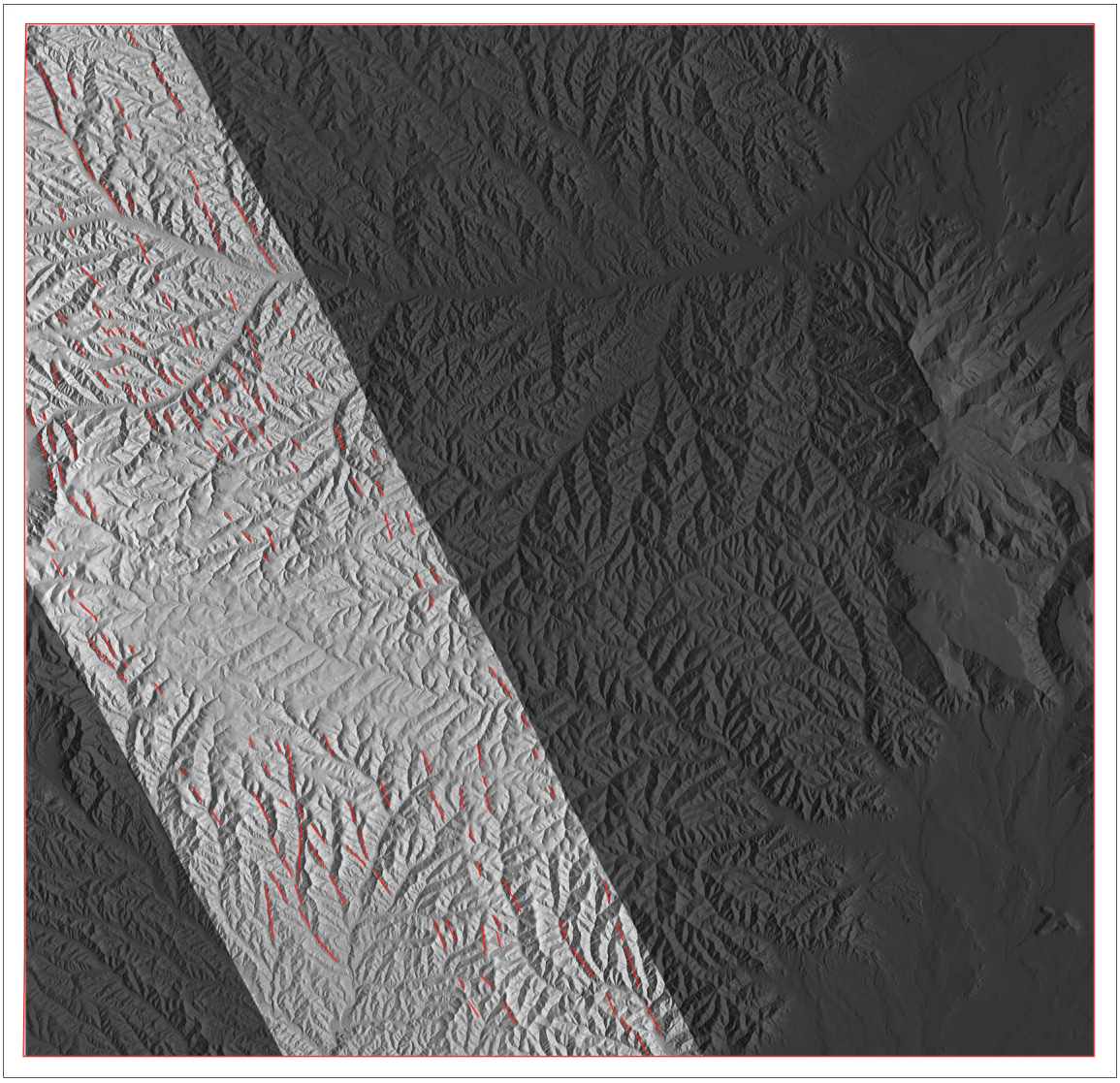

Figure A6. 200706091045A nodal plane 1. Dip direction 63° and dip angle 48°.

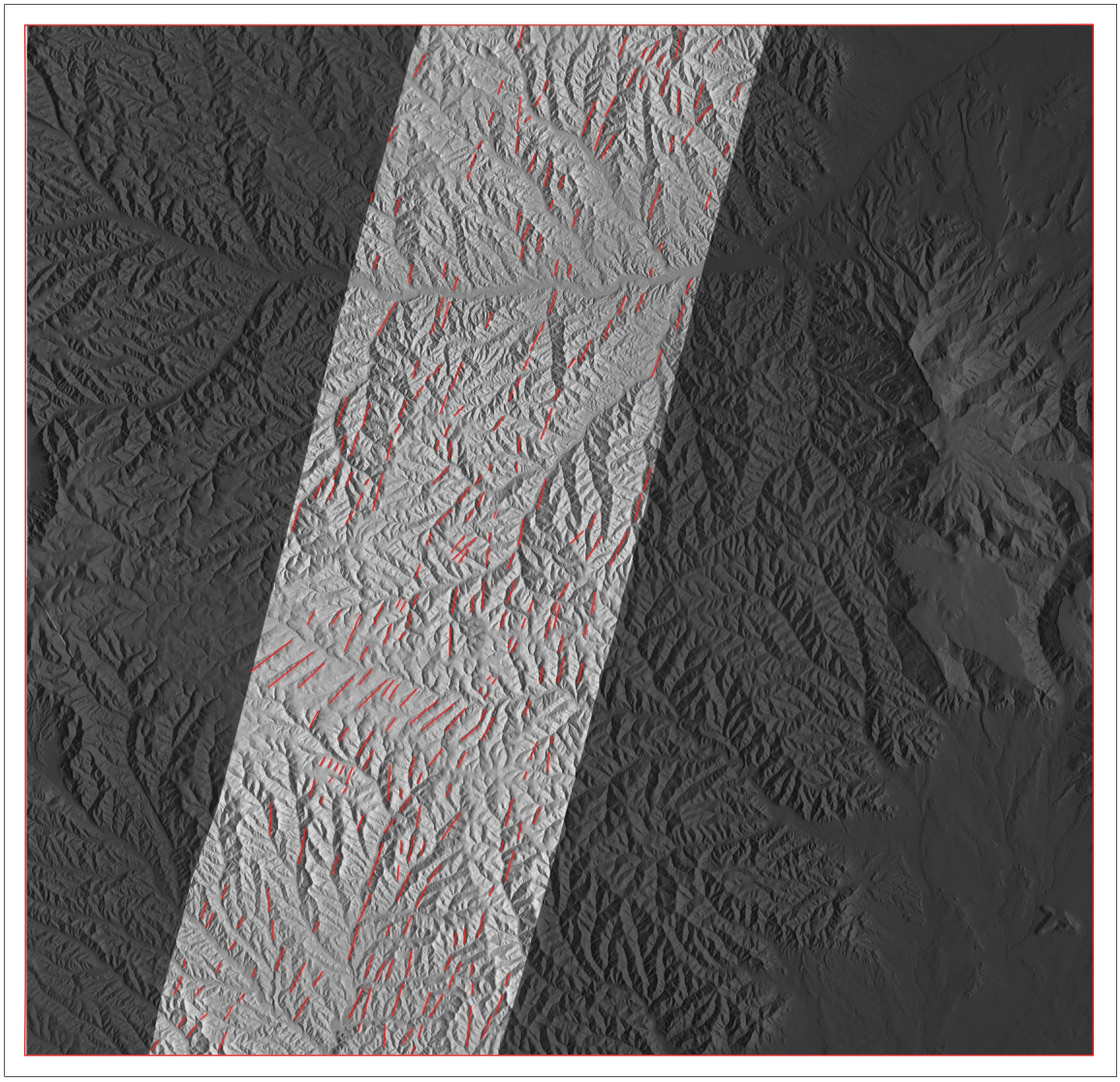

Figure A7. 200706091045A nodal plane 2. Dip direction 285° and dip angle 50°.

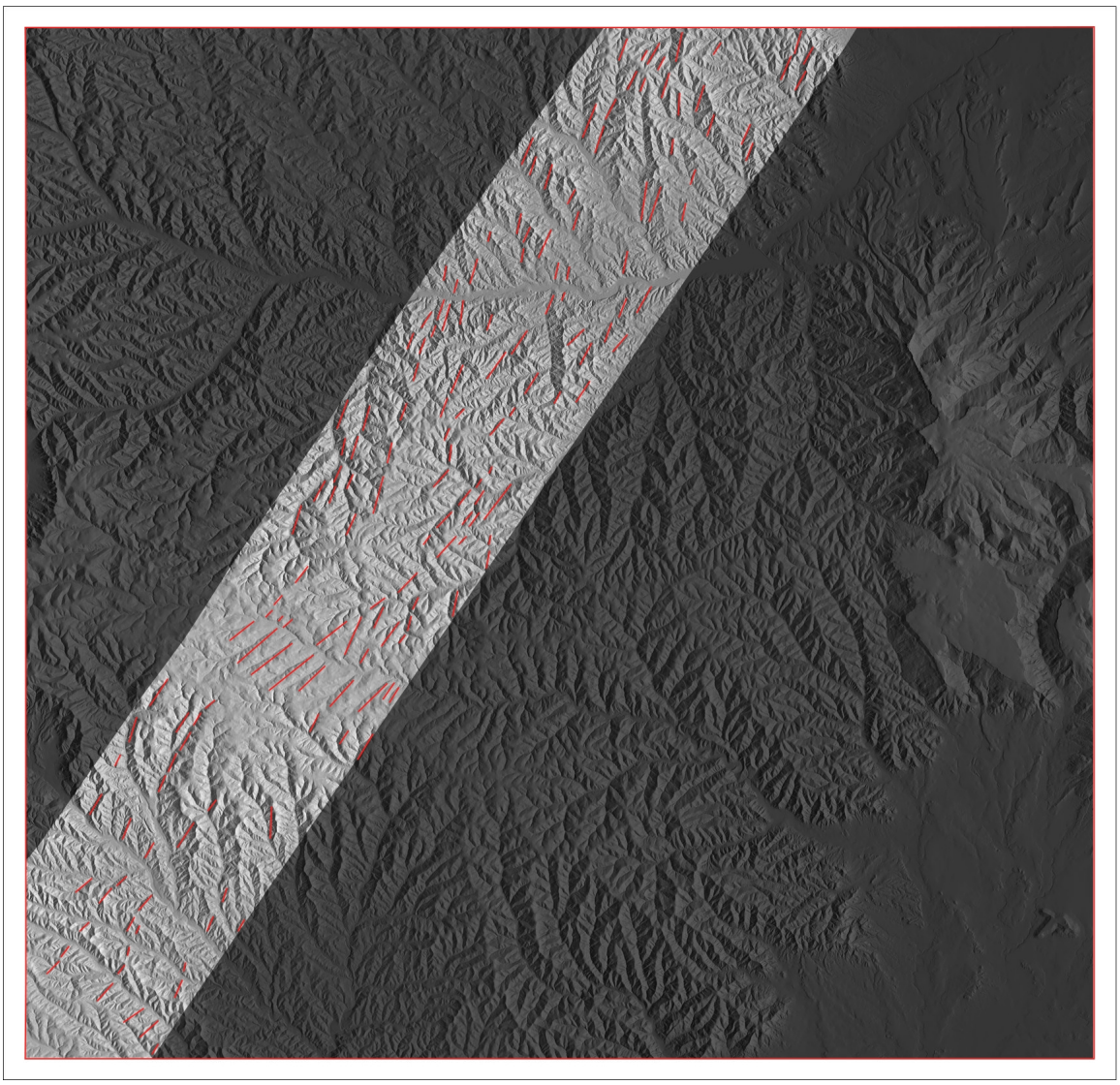

Figure A8. 201105092328A nodal plane 2. Dip direction 305° and dip angle 45°.

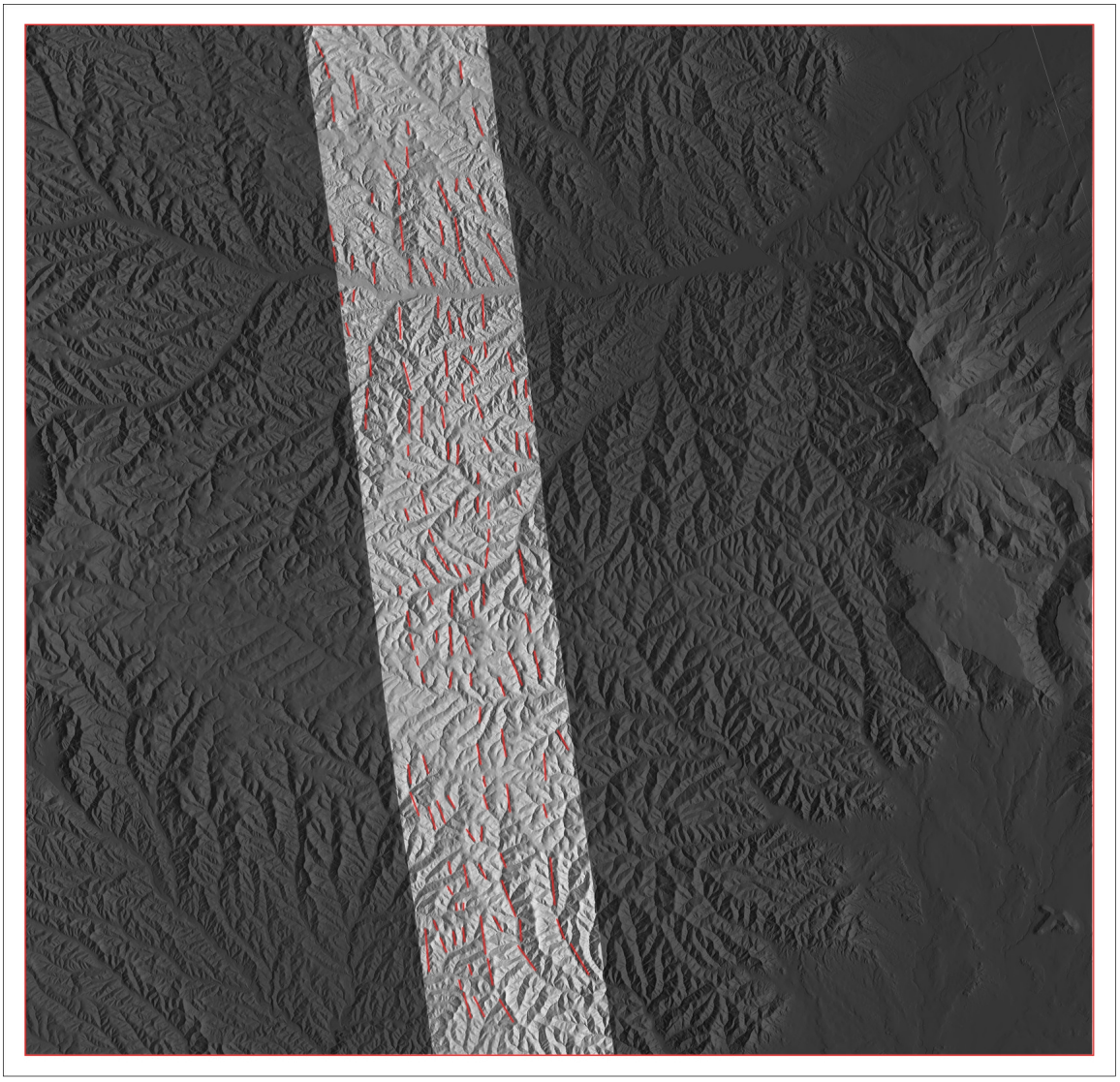

Figure A9. 201108222330A nodal plane 1. Dip direction 83° and dip angle 55°.

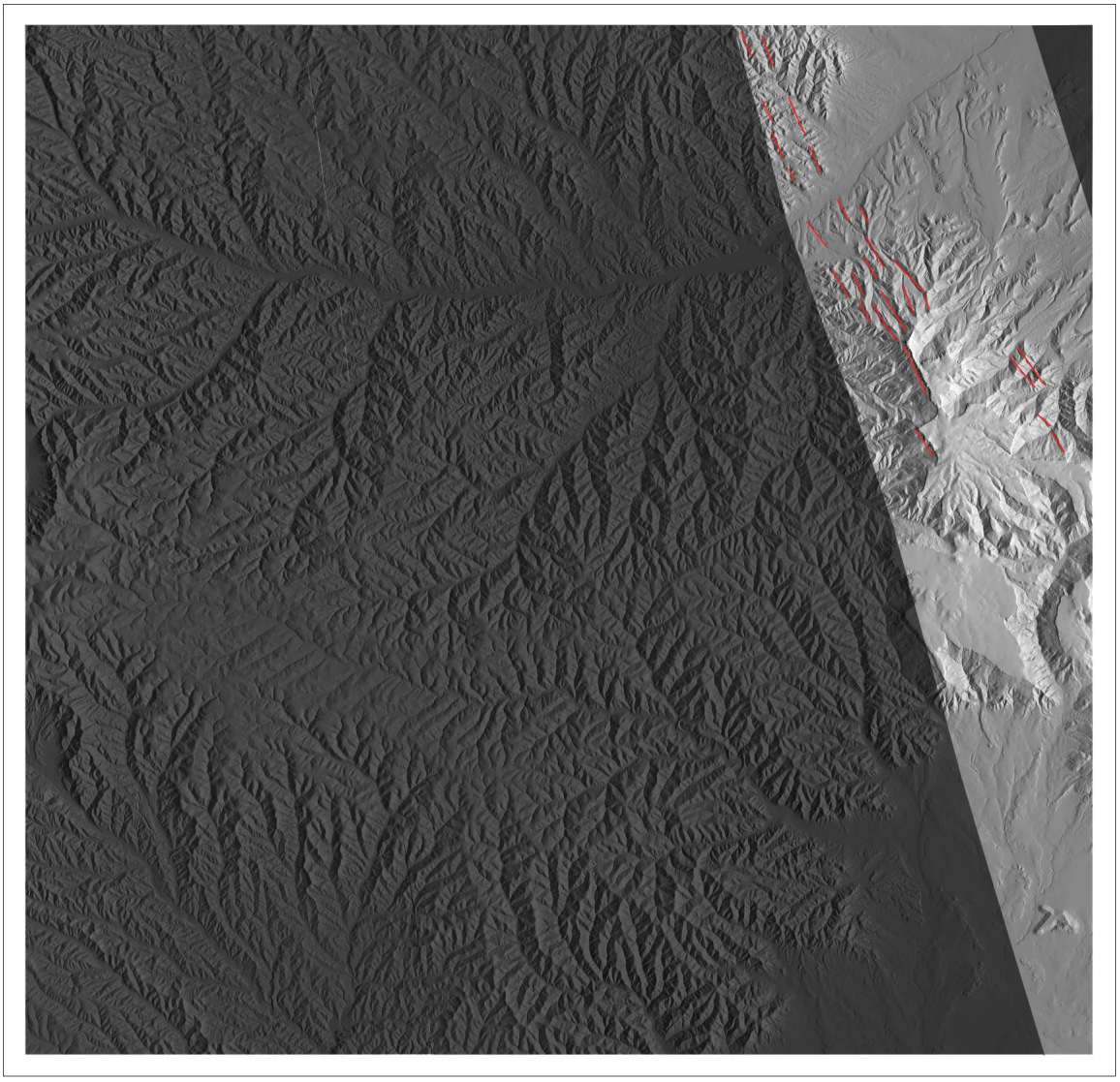

Figure A10. 201108222330A nodal plane 2. Dip direction 253° and dip angle 35°.

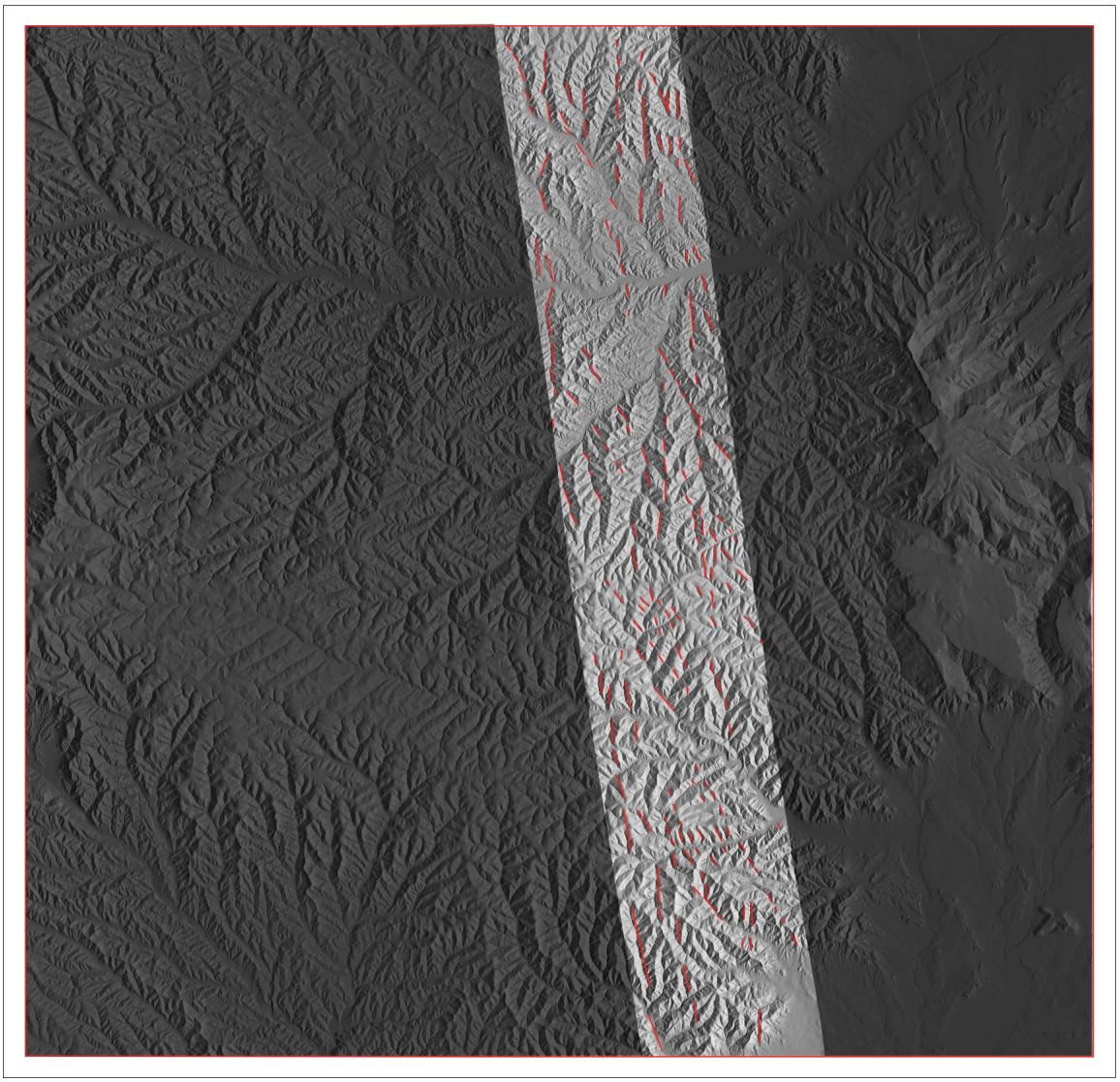

Figure A11. 201108222330B nodal plane 1. Dip direction 82° and dip angle 50°.

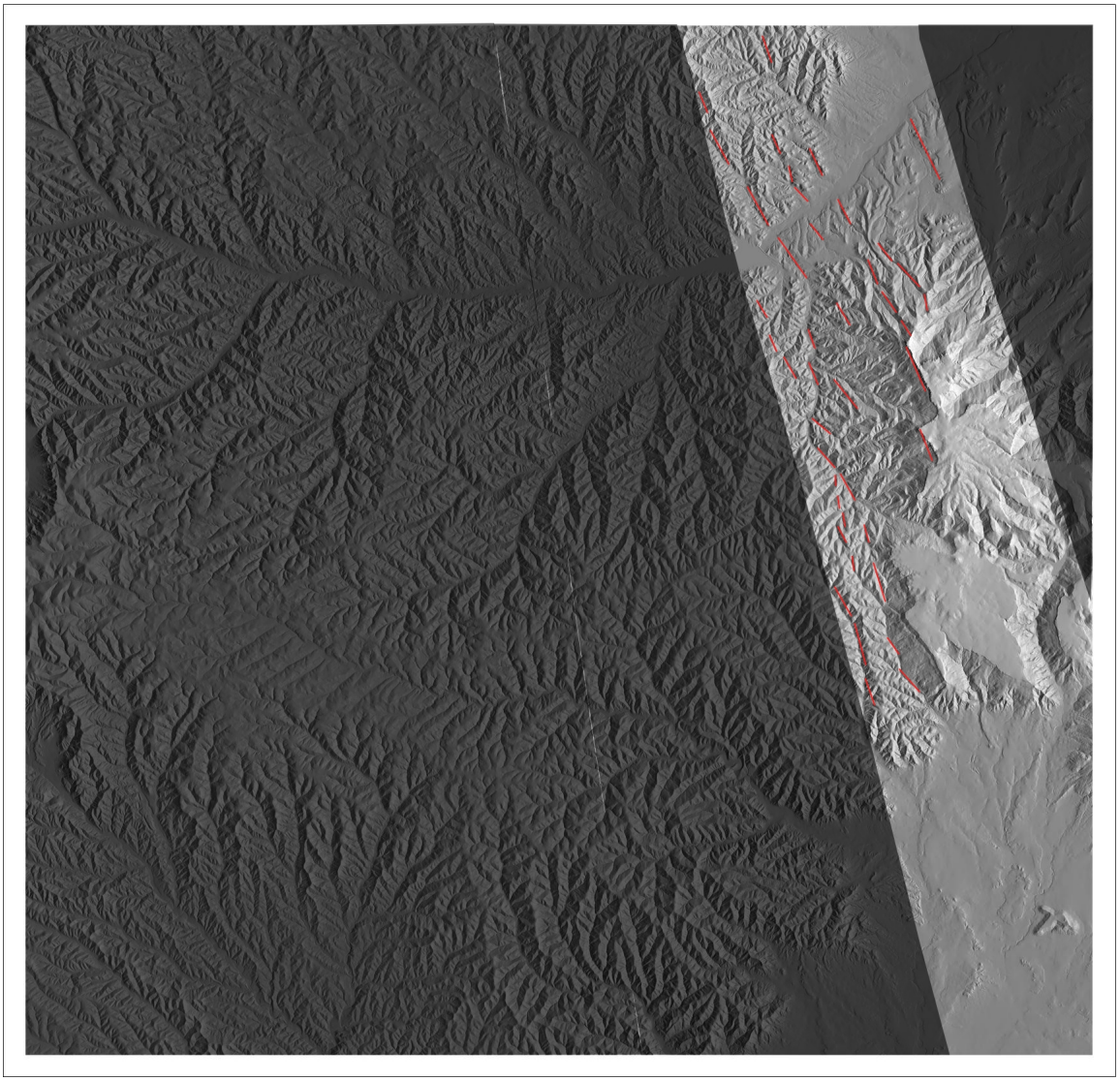

Figure A12. 201108222330B nodal plane 2. Dip direction 255° and dip angle 40°.

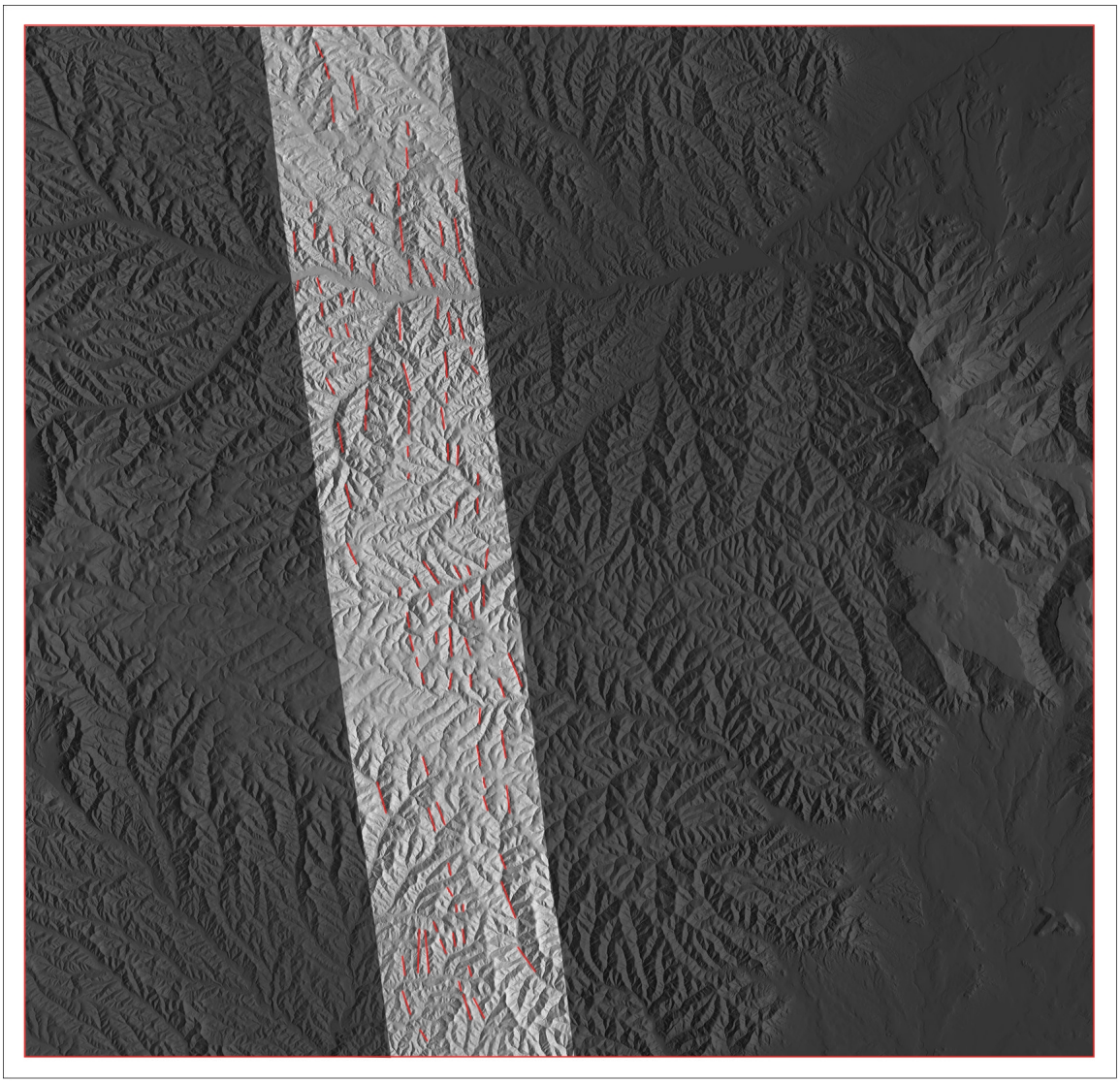

Figure A13. 201108222330C nodal plane 1. Dip direction 83° and dip angle 55°.

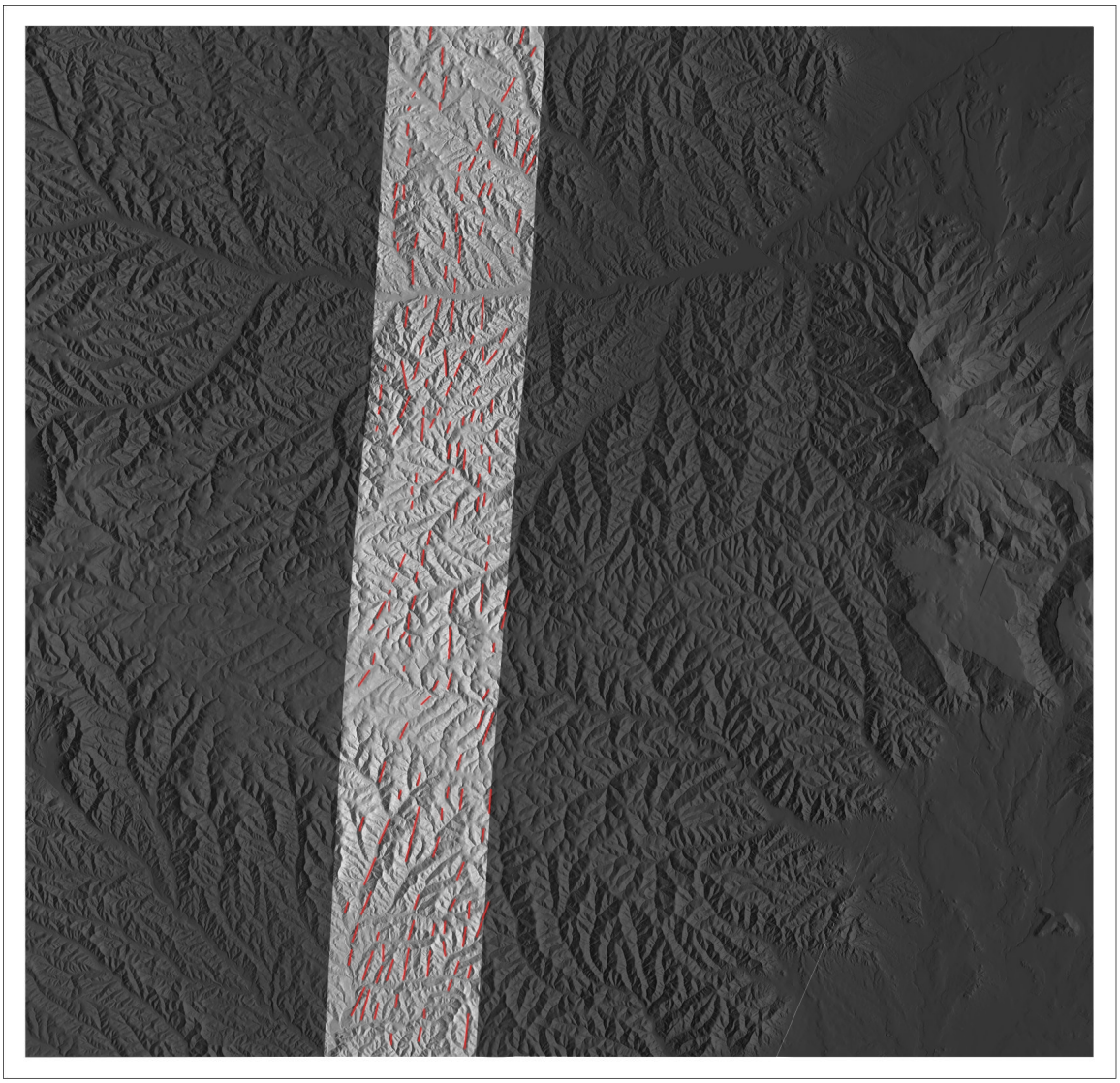

Figure A14. 201108230546A nodal plane 1. Dip direction 94° and dip angle 54°.

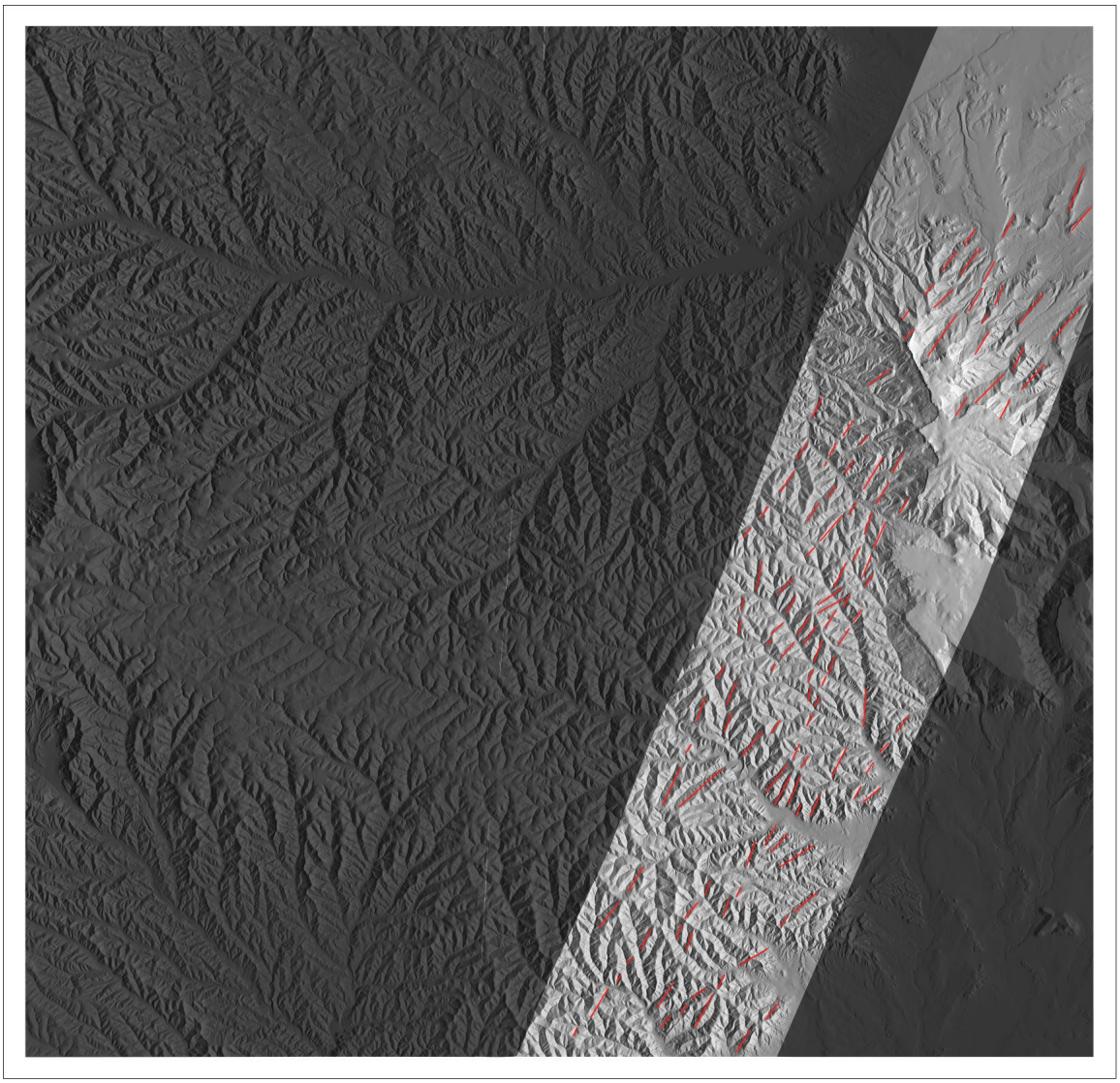

Figure A15. 201108230546A nodal plane 2. Dip direction 293° and dip angle 38°.

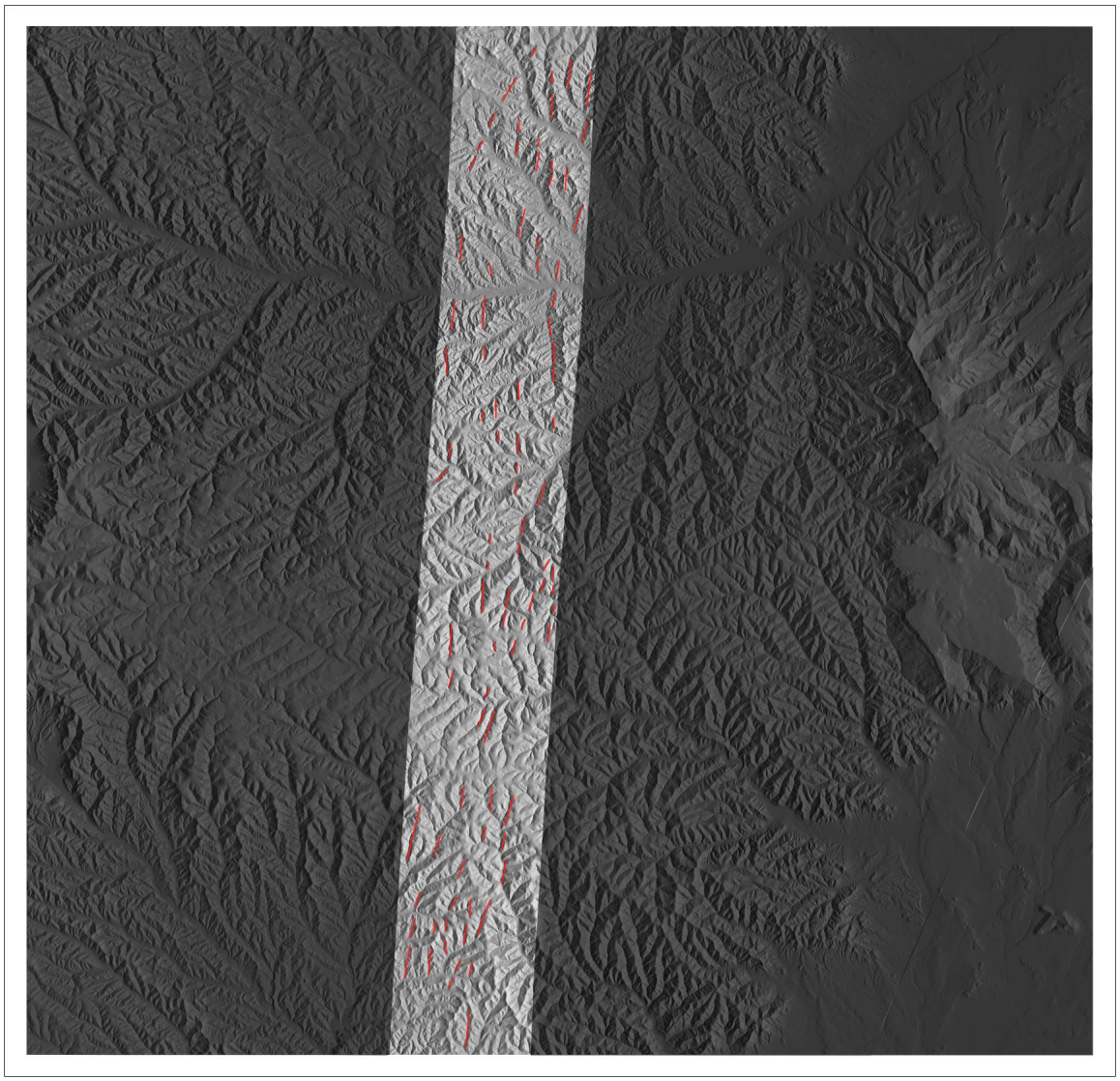

Figure A16. 201108230546B nodal plane 1. Dip direction 94° and dip angle 54°.

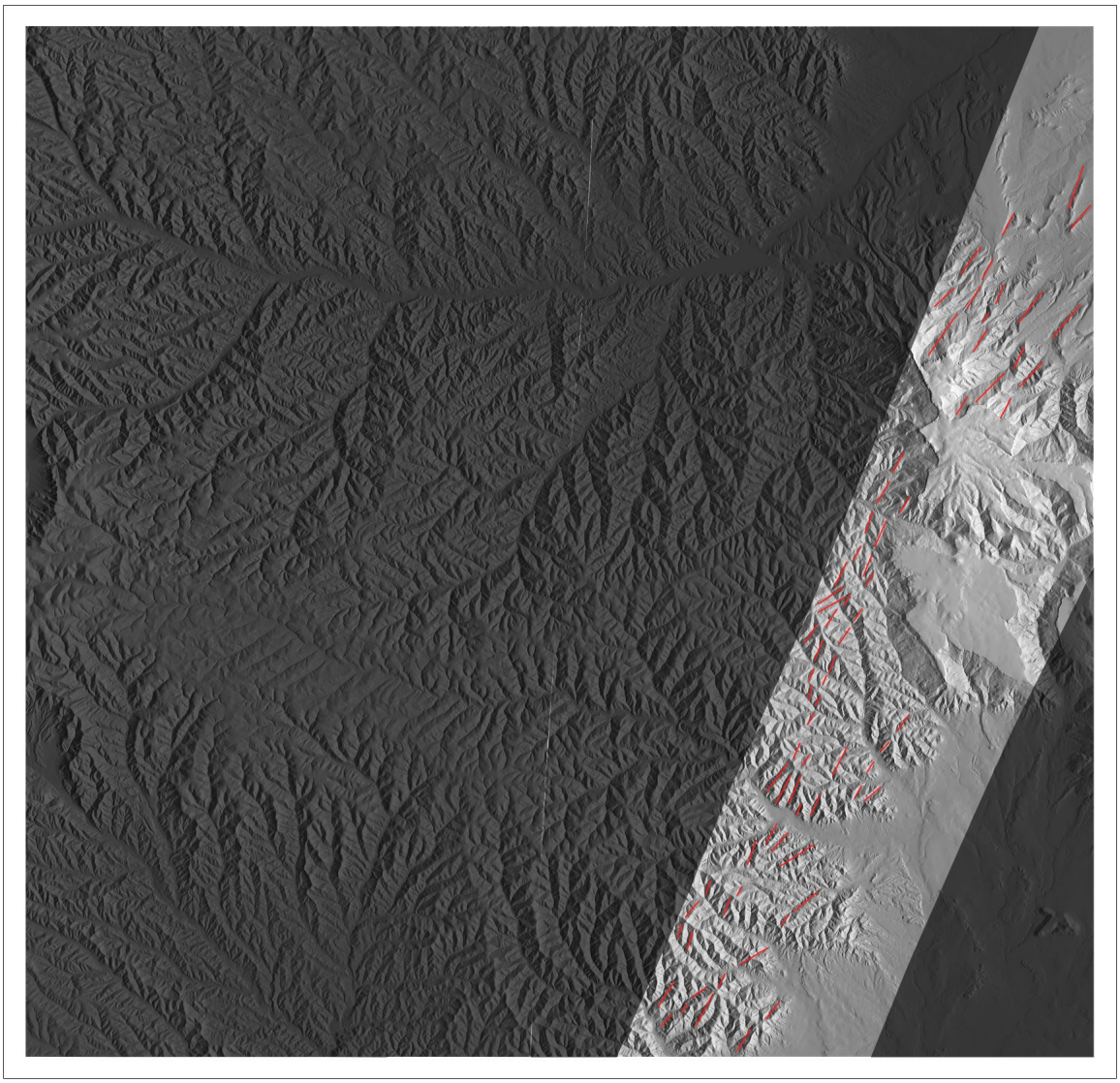

Figure A17. 201108230546B nodal plane 2. Dip direction 293° and dip angle 38°.

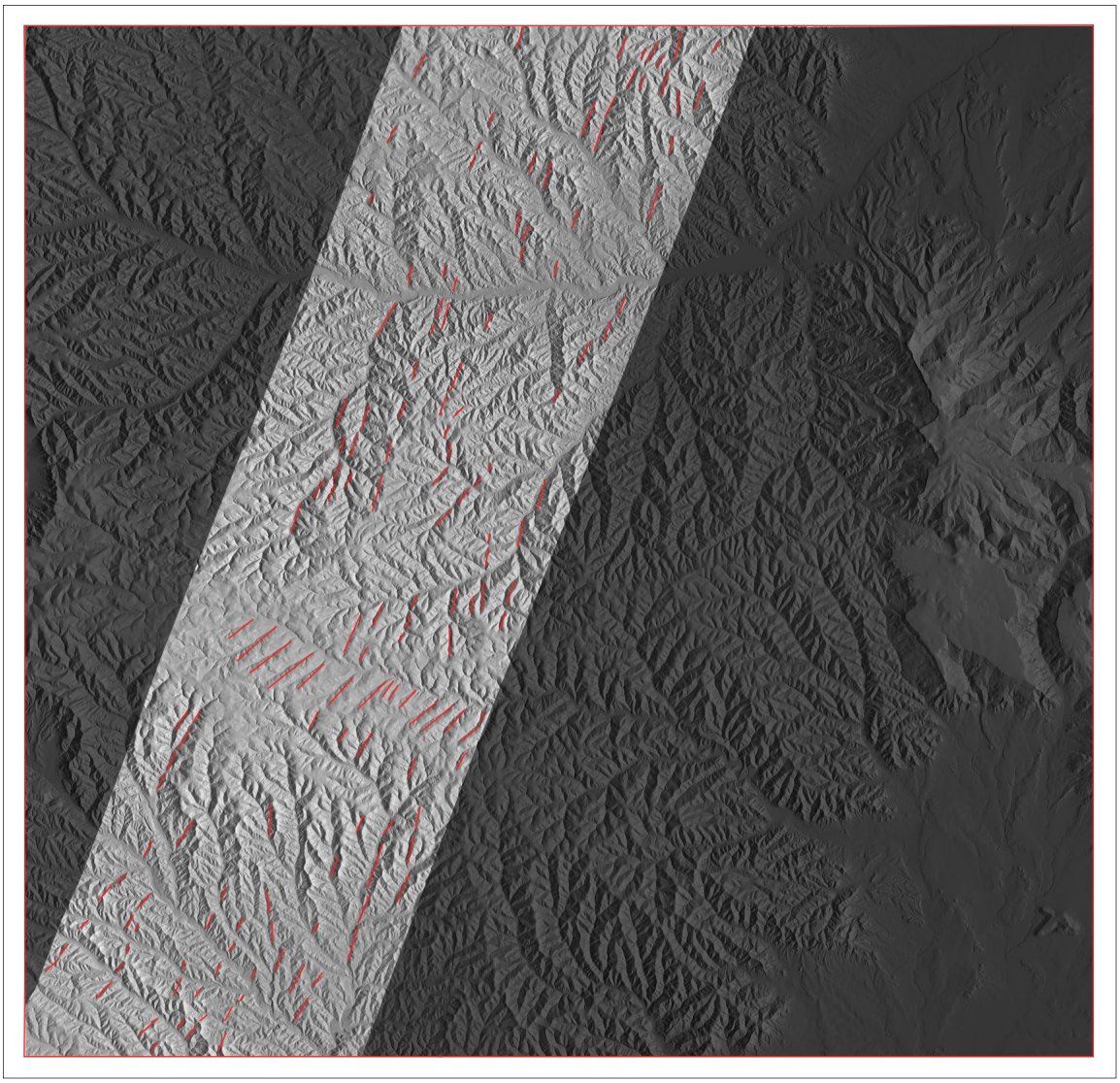

Figure A18. 201108230546C nodal plane 1. Dip direction 111° and dip angle 53°.

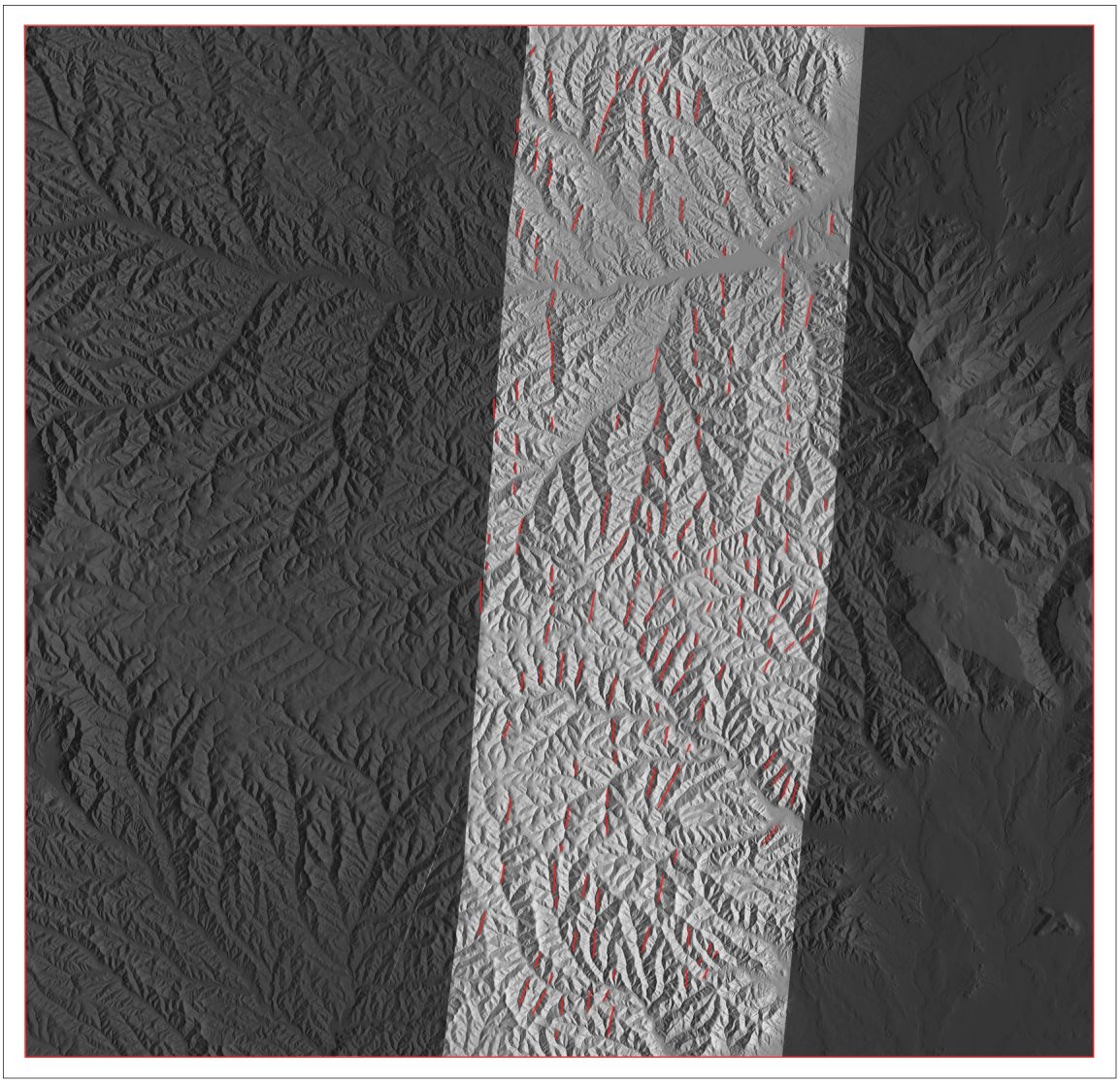

Figure A19. 201108230546C nodal plane 2. Dip direction 275° and dip angle 38°.

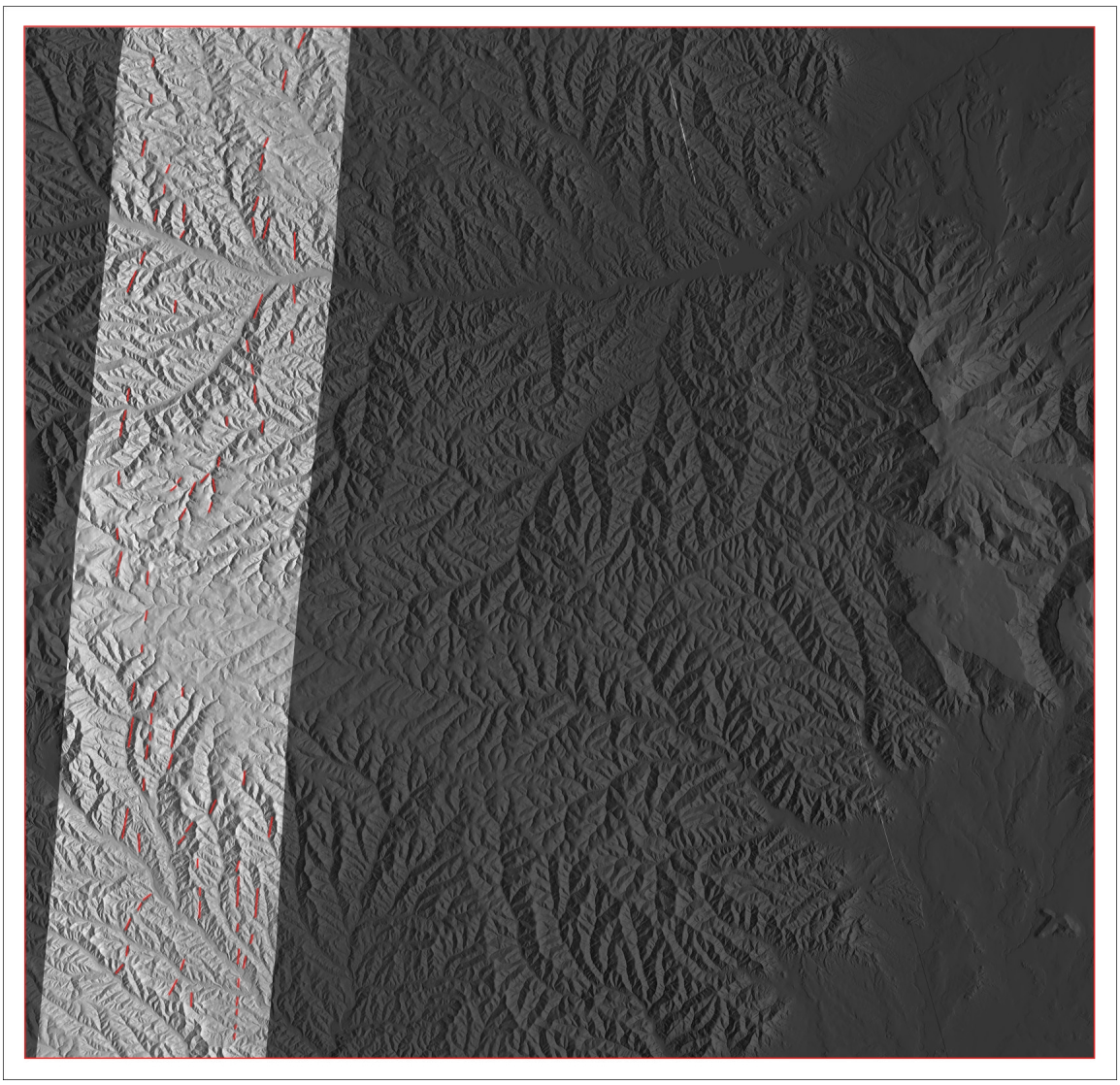

Figure A20. 201108231411A nodal plane 1. Dip direction 95° and dip angle 45°.

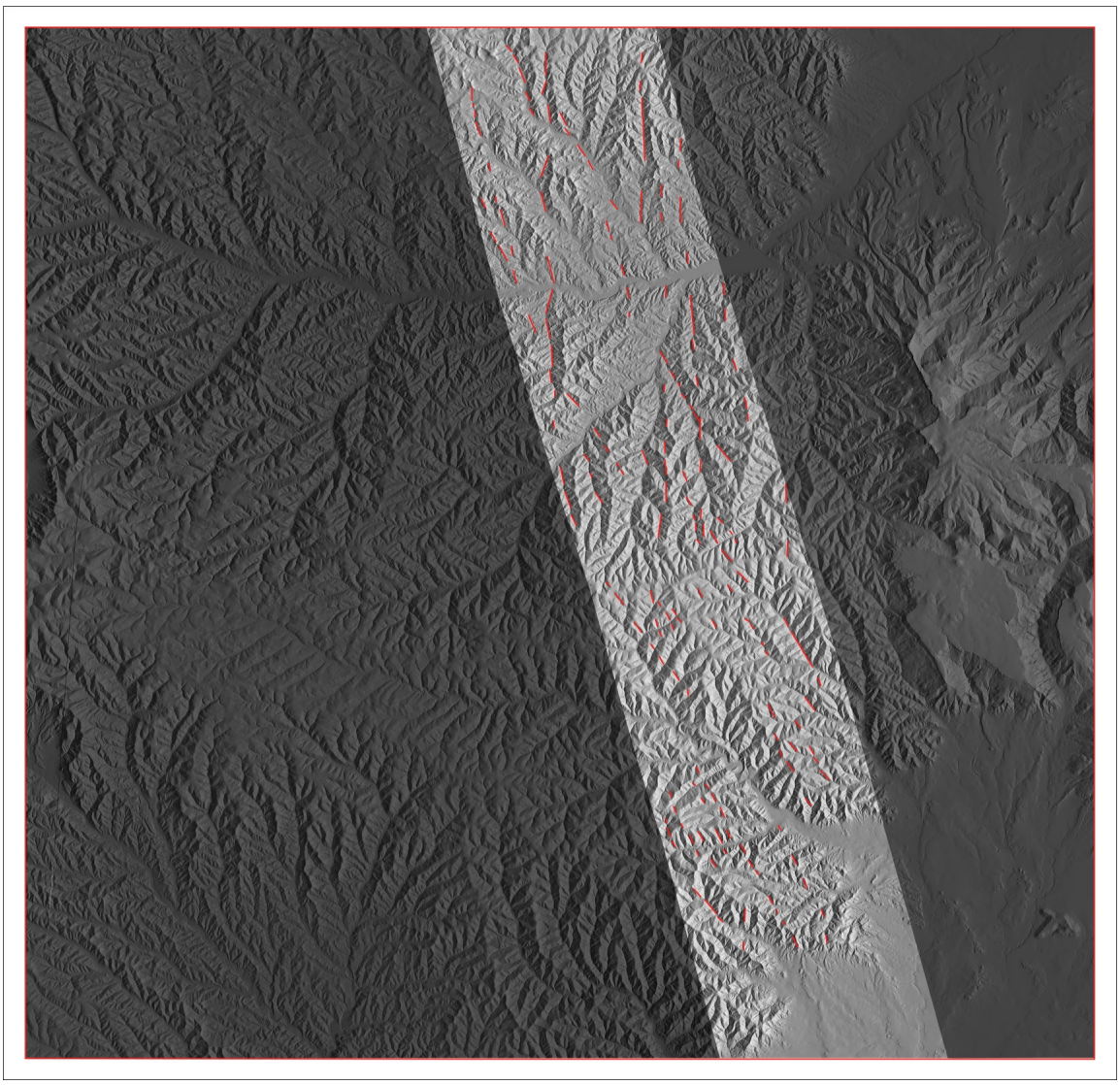

Figure A21. 201108231411A nodal plane 2. Dip direction 254° and dip angle 47°.

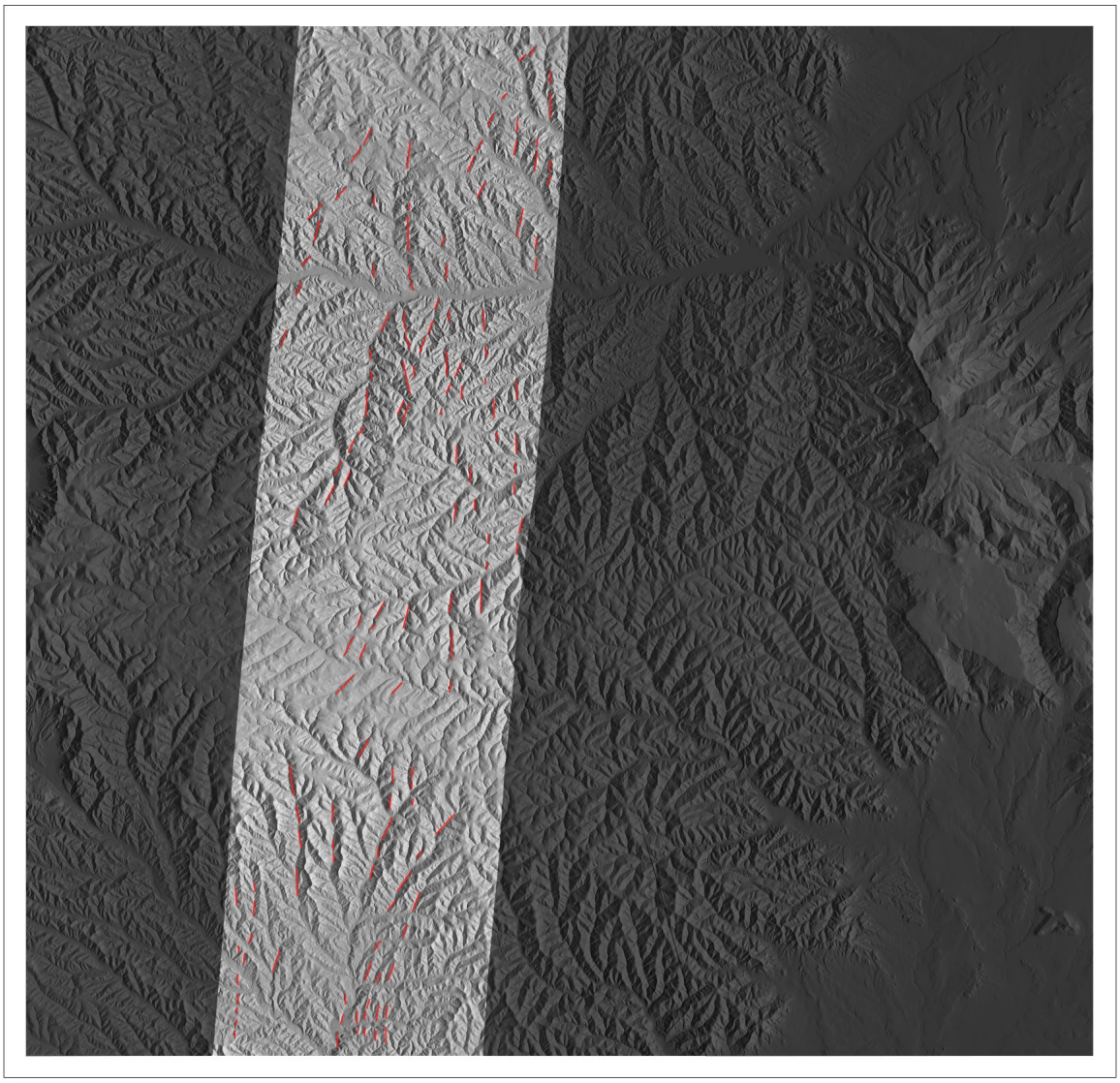

Figure A22. 201108231411B nodal plane 1. Dip direction 95° and dip angle 45°.

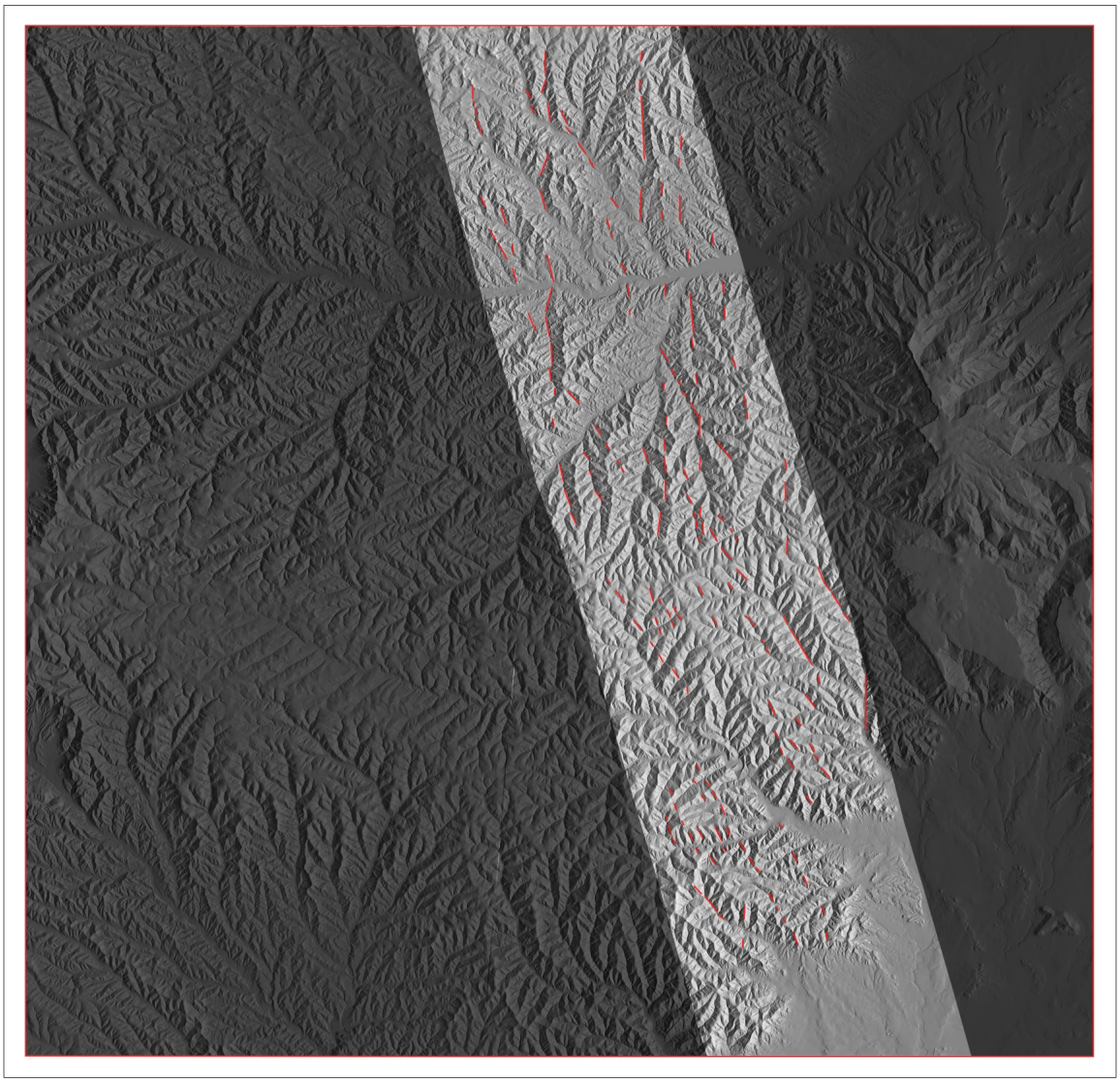

Figure A23. 201108231411B nodal plane 2. Dip direction 254° and dip angle 47°.